MLM-2927
NUREG/CR-2698
R 7

Aerosol Characterization from a Simulated HCDA: October 1976 — October 1981

William A. Zanotelli, Dale L. Roesch, and Gary D. Miller

July 7, 1982

Monsanto

MOUND FACILITY
Miamisburg, Ohio 45342

operated by
MONSANTO RESEARCH CORPORATION
a subsidiary of Monsanto Company

for the
U. S. DEPARTMENT OF ENERGY
Contract No. DE-AC04-76-DP00053

DISCLAIMER

Printed in the United States of America
Available from
National Technical Information Service
U. S. Department of Commerce
5285 Port Royal Road
Springfield, VA 22161

NTIS price codes
Printed Copy: A04
Microfiche copy: A01

MLM-2927
NUREG/CR-2698
R 7

Aerosol Characterization from a Simulated HCDA: October 1976 — October 1981

William A. Zanotelli, Dale L. Roesch, and Gary D. Miller

Issued: July 7, 1982

MOUND FACILITY
Miamisburg, Ohio 45342

operated by
MONSANTO RESEARCH CORPORATION
a subsidiary of Monsanto Company

for the
U. S. DEPARTMENT OF ENERGY

Contract No. DE-AC04-76-DP00053

Contents

1. Summary

Environmental conditions simulating the Hypothetical Core-Disruptive Accident (HCDA) on a reduced scale provided the following information:

- Aerosols resulting from the condensation of gaseous constituents without sodium generally comprise small, spherical, particles (diameter 0.01 to 0.25 μm) and branched chain-like structures.

- Aerosols resulting from the condensation of gaseous constituents with sodium generally comprise spherical, small (diameter 0.01 to 0.50 μm) particles, with some branched chain-like structures and some agglomerating particles.

Electron diffraction analyses identified actinide dioxides, fission products, fission product oxides, the constituents of stainless steel, sodium, an oxide of sodium (Na_2O), sodium uranates (Na_3UO_4 and Na_4UO_5), and the sodium plutonate compounds [Na_4PuO_5 and $Na_3(U,Pu)O_4$].

Reaction pathways are dictated by chemical kinetics rather than by thermodynamics, as the cooling process during which aerosols are formed from atomic species is a fast and essentially irreversible process.

Solubility studies show that for aerosols produced from laser vaporization of mixed oxide (U,Pu) pellets, 5.3% ± 1.5% of the plutonium-239 is water soluble, and 8.7% ± 2.4% of the plutonium-239 is water soluble when the aerosol is produced from a mixed-oxide (U,Pu) stainless-steel pellet vaporized in the presence of sodium.

Other solubility studies show that 2.6% ± 1.5% of the plutonium-239 is soluble in simulated lung fluid from an aerosol produced by vaporization of mixed-oxide (U,Pu), stainless-steel pellet, and 5.5% ± 1.1% of the plutonium-239 in the aerosol is soluble in simulated lung fluid when the vaporization is done in the presence of sodium.

The solubility of $^{239}PuO_2$ in sodium at 100 °C temperature increments from 500 °C to 800 °C ranged from 24.6 ±12.9 ppm to 48.0 ± 40.9 ppm.

The solubility of $^{239}PuO_2$ in sodium at 1000 ppm to 10,000 ppm oxygen impurity levels ranged from 20.9 ± 10.3 ppm to 38.6 ± 40.0 ppm.

There was no significant evidence that the solubility of $^{239}PuO_2$ in sodium was dependent on either temperature or oxygen level.

2. Introductory Overview

In support of the Nuclear Regulatory Commission, Mound Facility completed a program to produce and characterize the primary aerosols that could result from a hypothetical core-disruptive accident (HCDA) in a liquid metal fast breeder reactor (LMFBR). These tests were conducted under simulated conditions that can be related to the actual events that would occur under such a critical excursion.

The two main objectives of the study were: 1) the investigation of the chemical reactions and compounds formed from the short-lived vapor state existing in the HCDA event, and 2) the acquisition of a thermodynamic data base for the possible reactions and species formed from the interactions of the U-Pu-O-Na system.

The simulation of the HCDA event was accomplished by the laser evaporation technique. Mixed-oxide fuel (PuO_2/UO_2), stainless steel, and fission product materials were mixed and pressed into small pellets. Two systems, a static and a dynamic laser-heating system, were employed, with the dynamic system simulating the HCDA scenario more faithfully by providing a longer high-temperature-residence time.

In the static system, the pellet was placed on a heater on the pellet stand. The sodium, placed in a depression in the center of the pellet, was melted, and the focused laser beam was pulsed through the sodium liquid to the pellet. The vaporized aerosols from the

pellet and liquid sodium were condensed on Transmission Electron Microscopy (TEM) grids attached to Scanning Electron Microscope (SEM) stubs that were suspended from a copper fixture above the pellet.

In the dynamic system, the pellet was placed in a holder at the top of a quartz tube that was inductively heated. Heated sodium gas was introduced to the pellet and the focused laser beam was pulsed through the surrounding gas to the center of the pellet. The vaporized aerosols from the pellet, along with the sodium gas, were carried by an argon gas flow through the RF plasma. The aerosols and the sodium gas were condensed on TEM grids attached to SEM stubs which were attached to a copper fixture located below the RF plasma. The TEM grids were photographed and analyzed for particle size, shape, and morphology. Electron diffraction patterns were analyzed for compound formation.

The aerosols from the simulated HCDA were spherical and ranged in size from 0.01 to 0.50 μm. The branched chain-like particles, which are typical of mixed-oxide aerosols, have been verified. The combination of sodium with fuel to form sodium uranates and sodium plutonates was observed. There was no evidence that fuel and fission products react to form compounds under these conditions.

Aerosols were collected from the static laser system both with and without sodium for solubility studies in both distilled water and simulated lung fluid. In both cases increased solubility of plutonium-239 in the presence of sodium was observed.

The solubility of $^{239}PuO_2$ in sodium was studied at various temperatures and oxygen impurity levels. Neither temperature nor oxygen impurity level had any effect on the solubility of $^{239}PuO_2$ in sodium.

The principal use of the resulting data is for reactor safety analysis. The data are being compared with theoretical and existing analytical data and coordinated with other groups that have developed or are developing models from aerosol data. The models are used to assess the risk factors for the escape of radioactive aerosols from the reactor to the environment during an HCDA in a LMFBR.

3. The HCDA

3.1. Introduction

In support of the Office of Nuclear Regulatory Research, Nuclear Regulatory Commission, Mound Facility has established a program to produce and characterize the primary aerosols that could result from a hypothetical core-disruptive accident (HCDA) in a liquid metal fast breeder reactor (LMFBR). These tests were conducted under simulated conditions that can be related to the actual events that would occur under such a critical excursion. The program includes the following:

- A feasibility study to determine the possibility of direct acquisition of kinetic information regarding the chemical reactions for the U-Pu-O-Na system in the simulated HCDA environment.

- The acquisition of a thermodynamic data base of the possible reactions and species formed from the interactions of the U-Pu-O-Na system.

- The simulation of an HCDA event by the laser evaporation technique.

- The investigation of the chemical reactions and compounds formed from the short-lived vapor state existing in the HCDA environment.

- The assessment of the role of reaction kinetics on both the bubble formation and post-HCDA environment effects on the materials present throughout this accident sequence.

The resulting data are being compared with theoretical and existing analytical data and coordinated with other groups that have

developed or are developing models and aerosol data. Large amounts of experimental data exist on the generation and behavior of single-component aerosols, and some limited data exist on aerosols containing both uranium and sodium oxides, but little or no data exist on multicomponent systems containing aerosols generated from $(U,Pu)O_2$, sodium, and stainless steel produced under HCDA conditions.

Mound designed and fabricated a system that was capable of incorporating all these materials in a laboratory-scale simulation of an HCDA. The operation of a laboratory-scale simulation has enabled Mound to vary the operating parameters and materials.

3.1.1. The HCDA Scenario

During the most severe hypothetical core-disruptive accidents (HCDA) caused, for example, by transient overpower (TOP) or loss of flow (LOF), substantial amounts of the reactor fuel, stainless-steel cladding, and sodium coolant could be vaporized. The vapor species formed, including PuO, UO, PuO_2, UO_2, UO_3, O, O_2, Na, stainless steel, and the fission products, are expected to be contained initially in gas bubbles within the sodium coolant. A temperature gradient within the bubble will exist, initially, from probably greater than 2800 °C in the gas phase to about 900 °C at the liquid sodium walls of the bubble. As the bubble moves away from the primary heat source, cooling will cause condensation and reactions will occur at the liquid sodium walls of the bubble.

The physical and chemical nature of the aerosol particles is important in predicting the eventual behavior and fate of the aerosol. Physical properties of the aerosol (particle size, density, settling velocity, and coagulation tendencies) are currently being studied, chiefly by vaporization of UO_2. The chemical nature of the aerosol particles, which is determined by the chemical species present in the various temperature regimes transited by the aerosol, must be considered because it could affect the physical properties of the aerosol and would definitely influence the subsequent environmental and biological pathways of any aerosol that might escape from the reactor containment structure.

3.1.2. Literature Survey

Melting, vaporization, and release of fuel have been postulated to occur primarily following two low-probability hypothetical core-disruptive accidents (HCDAs): Loss of Flow (LOF) and Transient Overpower (TOP). It should be emphasized that these low probability HCDAs would occur only if one does not SCRAM the reactor. Since the reactor would SCRAM, and the fuel rods would be neutralized, the probability that an HCDA would occur due to an LOF or TOP condition is extremely low. Several computer models have been devised to predict different aspects of these accidents. Because of the differences in reactor designs, the complexity of the phenomena involved, and the uncertainties in the analysis, such "mechanistic" descriptions of the HCDA sequence of events vary somewhat [1-7].

In the LOF accident, when sodium flow has been decreased to about 25% of its normal value (after 4 or 5 sec), sodium saturation conditions are calculated to exist near the core outlet. Voiding the core selectively from the center channels outwardly causes positive reactivity feedbacks which result in steadily increasing power over a period of about 1 sec. Prompt criticality then increases the power level by several orders of magnitude, resulting in core self-disassembly. The resultant fuel motion is assumed to terminate the excursion. The specification of conditions that might exist in the core and in individual fuel elements just prior to the self-disassembly stage is uncertain. For example, peripheral fuel elements could still be under sodium, whereas central-region fuel elements could be dry or possess only a thin sodium film. The fuel elements with sodium and those with residual films may not contain significant internal melt fractions; whereas "dry" elements may have cladding melting, cladding removal by streaming sodium vapor or gravity, high fuel melt fractions, and fuel slumping. So, even without different accident sequences, diverse failure conditions could exist simultaneously in different regions of the core.

In the TOP accident, sodium is calculated to be in the core and the cladding and to remain

relatively cool while significant fractions of fuel are melted within the pins. Subsequently, the pins fail and molten fuel mixes with the sodium; the resultant fuel coolant interaction (FCI) causes sodium ejection. Resulting reactivity feedbacks produce a rapid excursion similar to that of the LOF.

The disassembly of the core and melting of the cladding are assumed to occur when the fuel reaches a temperature of 5000 K or greater. At these temperatures, gaseous fuel species and fission product oxides become the principal contributors to the vapor pressure. In LMFBR technology, the gaseous fuel species are the primary concern because the fuel is the main component of the reactor core. From the studies cited [8-12], it can be assumed that a pressure of about 100 atm is exerted by fuel at the 5000 K vaporization of the cladding. Pressures of 253 and 269 atm are predicted for 6000 K, and pressure of 1000 atm or greater are predicted for 7000 K [13]. In summary, these pressures exerted at the various temperatures cause the vaporization of the cladding containing the fuel and, thus, release the vaporized and molten fuel for interaction with the sodium coolant.

The fuel-coolant reaction is an important aspect of the analysis of HCDAs. In the early study, violent interactions were obtained when small quantities of sodium were injected into large amounts of inductively melted UO_2, and severe explosions resulted [14]. These explosive reactions were thought to be possible in an HCDA; however, large scale coherent UO_2 sodium vapor explosions appear impossible in a reactor environment [15]. In a real reactor system, fission gases and fragments, as well as solid materials and gas bubbles entrained in the liquid sodium, would be present and would promote boiling prior to reaching the threshold for homogeneous nucleation in sodium; mild interactions of the type observed in the Treat in-pile experiments would be the result [15].

The HCDA bubble consists of vapor species of fuel, sodium, stainless steel, and fission products. The HCDA bubble will be contained within the sodium coolant. A temperature gradient within the bubble will be 3073 K in the gas phase to 1173 K at the liquid sodium walls of the bubble [16,17,18]. The pressure exerted by the HCDA bubble has been calculated at approximately 19 atm [23]. This is the best estimate of conditions of the HCDA bubble after core disassembly and interaction with the sodium coolant.

When the HCDA occurs, temperatures of 3000 K and 6000 K are generated before the formation of the fuel bubble at equilibrium conditions of 3073 K in the aerosol and 1173 K at the sodium surface. Between 3000 K and 6000 K, the reactions predicted from the thermodynamic data are as follows: (1) the fuel will produce the oxides, UO, UO_2, UO_3, PuO and PuO_2, and O and O_2; (2) the sodium vaporizes into elemental Na; and (3) the stainless steel vaporizes into elemental Fe, Cr, and Ni [16-19]. As the temperature decreases from 6000 to 3000 K, the free energies for UO and PuO decrease, and the free energies for UO_2, UO_3, and PuO_2 increase, making these the dominant species. The pressures of free O and O_2 decrease as more UO_3 is produced. The stainless steel (Fe, Cr, and Ni) and elemental Na remain in a vapor state.

At the aerosol temperatures from 3000 to 1173 K, the dominant species remain UO_2, UO_3, and PuO_2 with minor combinations of UO and PuO present. The free O and O_2 pressures decrease as the O/M ratio increases. The available O and O_2 combine with Na and fuel to form Na_3UO_4 and $Na_3(U,Pu)O_4$ at temperatures between 1175 and approximately 1500 K in the vapor phase and continue in the liquid phase to 775 K [20-24]. Since the fuel originally contains more uranium than plutonium and since the thermodynamic properties are very close for both products, the probability is greater that Na_3UO_4 will be the dominant specie over $Na_3(U,Pu)O_4$. At this point, the oxygen pressures are very small and, for all practical purposes, used up. If any appreciable oxygen is left, it could form oxides with stainless steel (Fe, Cr, and Ni) which is highly unlikely. If oxides are formed, the free energies of formation predict $Cr_2O_3 > Fe_3O_4 > NiO$. Since no literature can be cited to support this assumption, it is likely that the Fe, Cr, and Ni condense as fine elemental particles.

In summary, it is assumed that the cool-down products of the HCDA aerosol bubble are UO, UO_2, UO_3, PuO_2, Na_3UO_4, $Na_3(U,Pu)O_4$, and elemental Fe, Cr, and Ni. These predictions are estimated with no contributions from fission products considered.

The magnitude of the plutonium aerosol source term used in estimating plutonium transport to the environment in the event of a large core-disruptive accident in an LMFBR is still poorly defined. The most important source will likely result from condensation of fuel that has been vaporized during the accident. Sizes for condensed fuel particles prior to agglomeration are less than 1.0 μm [25].

In an HCDA, the bubble components will condense into an aerosol composed of PuO_2 and UO_2 mixed with sodium. The particle size distribution was estimated to range from 0.10 to 0.38 μm [19].

Large particles, such as those produced in fuel-sodium interactions, would tend to settle out rapidly before leaking from the containment [25,26]. A particle size distribution was reported for an HCDA bubble containing two-phase sodium and UO_2-PuO_2 fuel in the form of an aerosol [26]. The particle distribution was divided into 11 sizes, with 2% of the mass having a diameter of up to 10 μm; 8% with a diameter of up to 30 μm; and the other 90% of the mass being equally divided into diameters of up to 60, 110, 160, 225, 310, 500, 850, 1450, and 2500 μm [26,27], indicating that particles greater than 10 μm result from a fuel-coolant reaction. It is not clear, however, what happens to stainless steel while the bubble is rising, since the condition (e.g., the particle size distribution) of molten steel at the end of the fuel-coolant interaction is not known [26]. Stainless steel did not appreciably alter the total amount of fuel that leaked to the secondary containment. Leakage values for two flow areas through the cover were 2.2% and 10.1% with steel and 2.1% and 9.6% without steel where lower values correspond to 0.1 ft^2, and higher values correspond to 1.0 ft^2 [26], condensing on the branch chain structures and forming the more complex aerosol particulates [28]. This effect would be the case if fission products reacted with the fuel species to form reaction products with the net result of larger and more complex particulates [28]. The minor products of Fe, Cr, and Ni from stainless steel would also form larger particles than would the oxide reaction products [29].

In summary, the reaction products formed from the cool-down of the HCDA bubble should have particle size distributions equal to or greater than 10 to 2500 μm. These are the values for the UO_2-PuO_2-Na interactions which form the aerosols in the HCDA bubble [26]. These predictions are based on the assumption that fission products are not considered as part of the interaction system and have been ignored.

3.1.3 HCDA Simulation Methods

Three HCDA simulation methods were used for these studies: the capacitance discharge system, the static laser system, and the dynamic laser system.

The capacitance discharge system consisted of a quartz tube with high-voltage leads which contained a stainless-steel fuel pin filled with UO_2 and $Na_2U_2O_7$ fuel. The tube was placed inside a set of RF coils, and an RF plasma was generated with argon gas. The simulation was accomplished when sodium gas was introduced into the quartz tube at the same time as the voltage was applied across the fuel pin, causing the vaporized fuel pin and sodium gas to mix and fall through the high-temperature RF plasma (>6000 °C). The vaporized particles were condensed on sample collectors and analyzed for compound formation and particle size.

The static laser system consisted of a ceramic-coated heater on top of a pellet stand that was centered inside a pyrex cylinder. The cylinder had entry and exit ports to purge argon gas and a quartz top. A fuel and stainless-steel pellet that contained sodium metal in a depression in the center was placed on the pellet stand. The simulation was accomplished when the heater melted the sodium, and a focused laser beam was pulsed through the sodium liquid into

the pellet, vaporizing the sodium and portions of the pellet at ~6000 °C.The vaporized particles were condensed on transmission electron microscope (TEM) grids that were attached to scanning electron microscope (SEM) stubs, which were suspended from a copper fixture above the pellet. The grids and stubs were analyzed for compound formation and particle size.

The dynamic laser system consisted of a quartz tube body and top that contained the pellet holder and entry ports for the argon and sodium gas. The quartz tube, containing a fuel and stainless-steel pellet, was placed inside of a set of RF coils, and an RF plasma was generated with argon gas. The simulation was accomplished when sodium gas was introduced into the quartz tube at the same time that the focused laser beam vaporized a portion of the pellet, causing the vaporized pellet and sodium to mix and fall through the RF plasma (>6000 °C). The vaporized particles were condensed on TEM grids attached to SEM stubs that were suspended from a copper fixture below the RF plasma at the bottom of the quartz tube. The TEM grids and SEM stubs were analyzed for compound formation and particle size.

3.2. Experimental

3.2.1. Capacitance Discharge Method

3.2.1.1. Apparatus and Procedure

In all phases of the study, stainless-steel fuel pins were heated by the capacitance discharge method. Figure 1 illustrates the quartz reaction chamber that was located in a glovebox. The capacitance fuel pin test used a 44-J capacitance discharge unit (CDU) with a discharge time of a few microseconds. The capacitor charge to the pin was 3000 V, and the energy available for pin firing was 450 J. The fuel pin preheat temperature was ≅700 °C. The argon flow rate was 6.6 x 10^{-4} m^3/sec, and the RF generator plate current was 1.0 A. The fuel was loaded into a 316 stainless-steel tube (fuel pin, 1.0 mm diameter by 0.05 mm wall thickness by 18.75 mm long), and the ends of the tube were pinched shut. The fuel pin was connected to the CDU leads inside the reactor chamber. The CDU test equipment was adjusted to the desired test parameters, and the fuel pin was exploded. Figure 2 illustrates the complete experimental setup used for these studies. The vaporized fuel pin, along with the sodium gas, is carried by an argon gas flow through the RF plasma and condensed on the sample collector as shown in Figure 1. The samples were analyzed for particle size using a Leitz Classimet Image analyzer. The samples were analyzed for compound formation by the Debye-Sherrer powder x-ray diffractometry method.

3.2.1.2 Systems Studied and Rationale

The materials used for this study were composed of depleted uranium dioxide (UO_2), sodium diuranate ($Na_2U_2O_7$), and thorium oxide (ThO_2) mixed to the following compositions (in wt %):

1) 20% UO_2-80% $Na_2U_2O_7$

2) 20% UO_2-80% $Na_2U_2O_7$

3) 20% UO_2-80% $Na_2U_2O_7$

4) 100% UO_2

5) 100% ThO_2

6) 100% UO_2

7) 100% UO_2

8) 100% UO_2

The UO_2 was prepared by reducing U_3O_8 in a hydrogen atmosphere and confirmed by x-ray diffraction to be UO_2. The $Na_2U_2O_7$ was precipitated with NaOH. The precipitate was washed with water to eliminate excess NaOH and then dried. The ThO_2 was 99% pure. The reactor structural material was 316 stainless-steel tubing. The sodium was reagent grade metal which was stored under xylene.

The materials were mixed using a mortar and pestle and loaded into 1.0 mm diameter by 18.75 mm long, 316 stainless-steel tube.

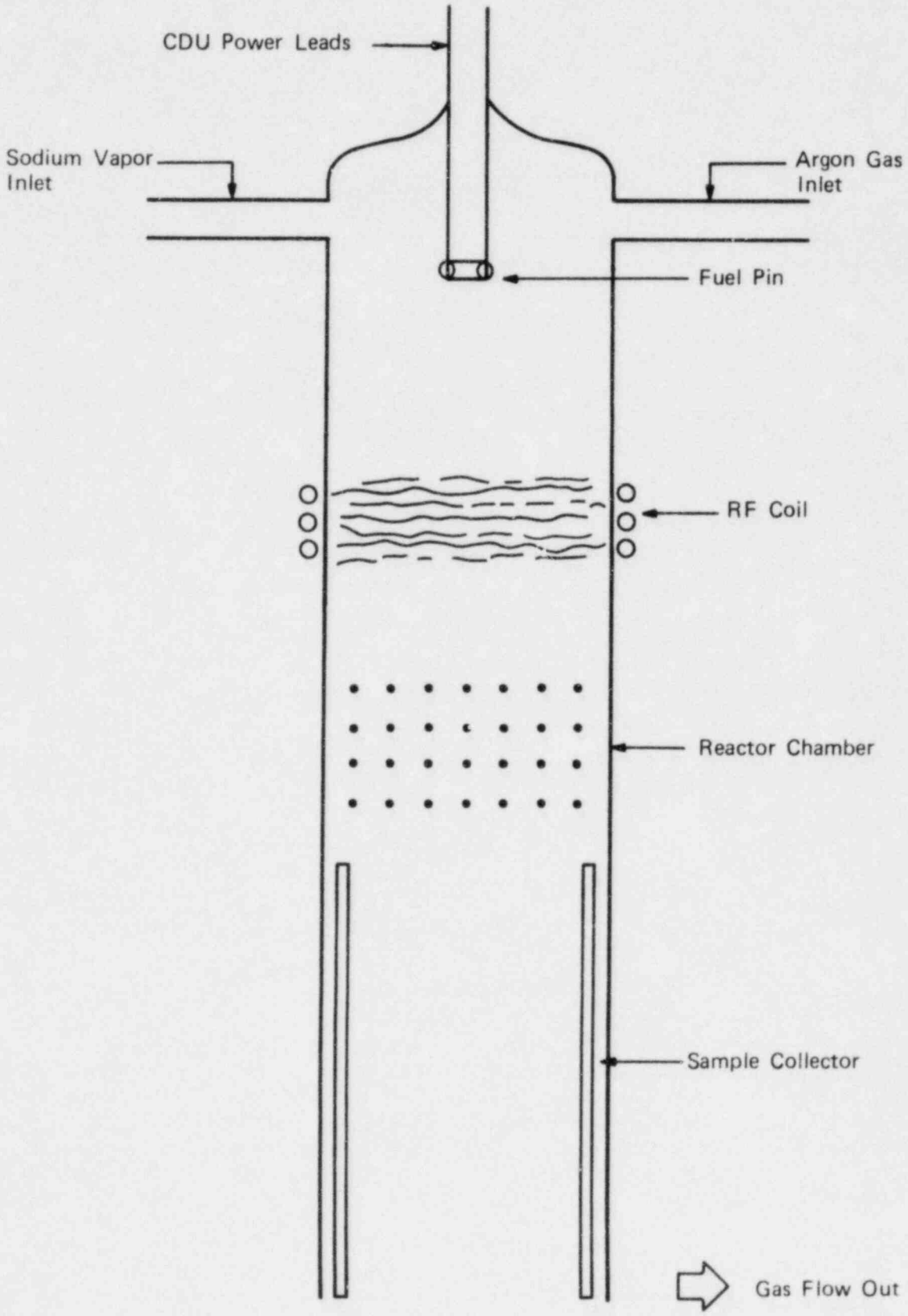

FIGURE 1 - Quartz reaction chamber.

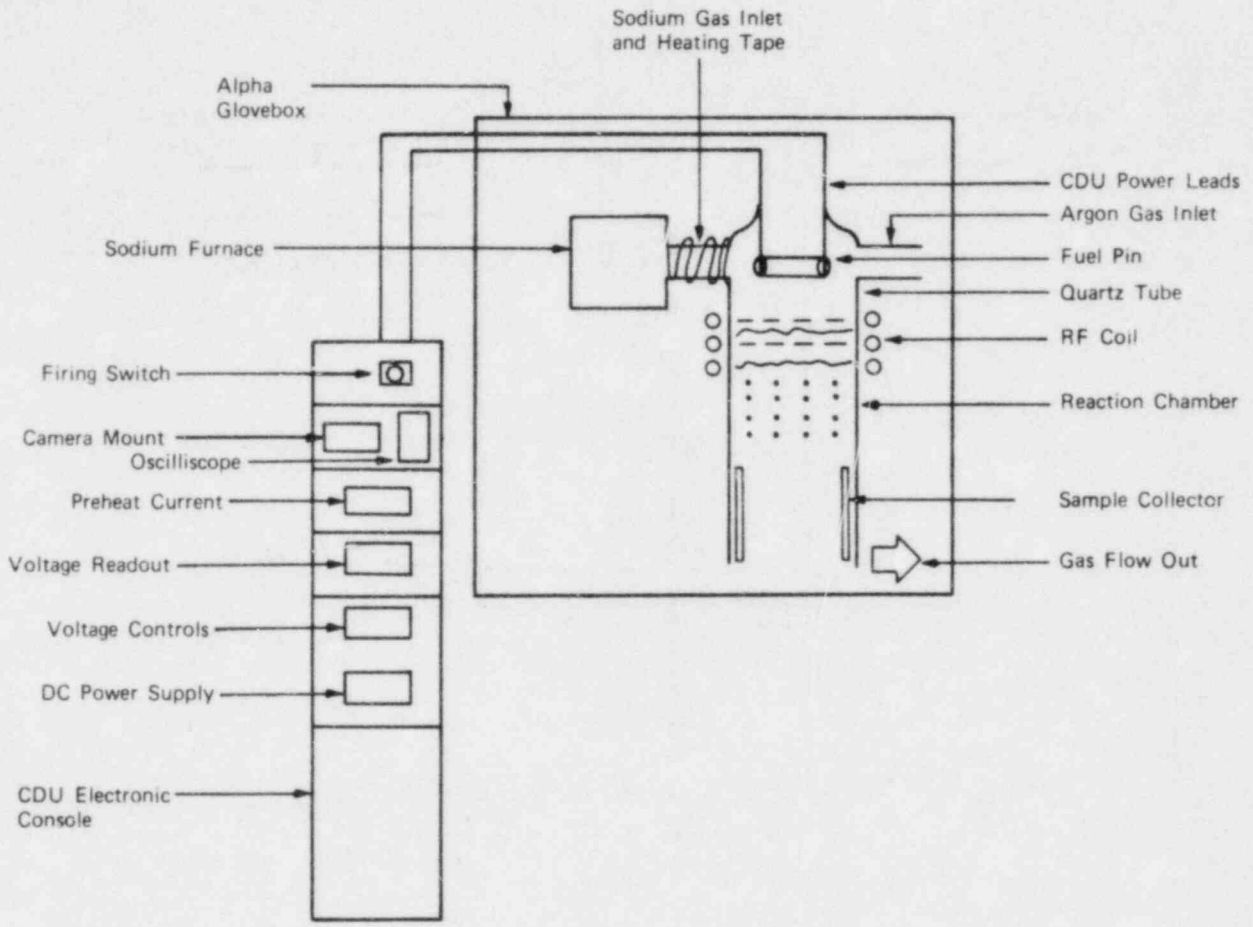

FIGURE 2 - Capacitance Discharge unit (CDU) experimental system.

This study was done to simulate the HCDA conditions using the CDU method and to acquire background information on particle size analyses and compound formation with UO_2 before introducing PuO_2.

3.2.1.3. Results

Results from the study by the CDU method were primarily assessed by examining the products by x-ray diffraction and particle size analyses. The pellet compositions, compounds identified, and particle size range data collected from the analyses are summarized in Table 1. The fuel pins that were heated by capacitance discharge (CD), with or without sodium, formed compounds that were not too different from the starting compounds (see Table 1). The compounds identified were U_2O_5, U_3O_8, U_4O_9, ThO_2, $Na_2U_2O_5$, and FeNi. The U_2O_5, U_3O_8, and U_4O_9 are superstoichiometric oxides of UO_2 and can be designated as $UO_{2.5}$, $UO_{2.67}$, and $UO_{2.25}$. These oxides are favored and are expected to

Table 1 - ANALYSIS OF EIGHT MODEL FUEL PIN FIRINGS

Sample No.	Fuel	Wt. Fuel Pin (g)	Wt. Fuel (g)	Wt. Residue (g)	X-Ray Diffraction Results	Particle Size Analysis (Size range in μm, % as particles)		Comments
1*	20% UO_2 80% $Na_2U_2O_7$	0.1345	0.0861	0.0951	U_4O_9 $Na_2U_2O_5$	—		No sodium vapor used
2*	20% UO_2 80% $Na_2U_2O_7$	0.1345	0.0862	0.0953	U_4O_9 $Na_2U_2O_5$ FeNi	—		No sodium vapor used
3*	20% UO_2 80% $Na_2U_2O_7$	0.1399	0.0905	—	U_4O_9 $Na_2U_2O_5$ Fe Ni	—		No weight on sample residue
4*	100% UO_2	0.1611	0.1131	—	U_4O_9 U_3O_8	—		No weight on sample residue
5*	100% ThO_2	0.1429	0.0483	—	ThO_2	—		No weight on sample residue
6*	100% UO_2	0.1648	0.1169	0.0567	U_4O_9 U_3O_8	—		Difficulty maintaining sodium vapor flow
7*	100% UO_2	0.1637	0.1153	0.0737	U_4O_9 U_3O_8	<5 5-10 10-15 15-20 20-25 25-30 30-35 35-40 40-45 45-50	37.4% 12.3 5.5 5.7 3.6 1.7 2.3 2.6 2.9 26.0	Difficulty maintaining sodium vapor flow
8	100% UO_2	0.1055	0.0563	0.0712	U_4O_9 U_3O_8	<5 5-10 10-15 15-20 20-25 25-30 30-35 35-40 40-45 45-50	32.4% 13.4 6.3 6.5 6.8 3.2 5.3 3.0 3.3 19.8	Maintained a good sodium vapor flow

*Designates samples formed from two fuel pin firings.

form from UO_2 at high temperature in an air atmosphere. The compound $Na_2U_2O_5$ was formed, at high temperature, as the decomposition product of $Na_2U_2O_7$. The compound ThO_2 was one of the starting compounds. The compound FeNi is a product formed from the two components of stainless steel, iron and nickel.

The particle size analyses data were collected on samples 7 and 8 (see Table 1). The greatest percentages of particles were smaller than 5.0 μm, 37.4% and 32.4%, respectively. For both analyses, 49.7% and 45.8% of the particles were <10.0 μm in diameter. The next greatest concentration of particles was in the 45-50 μm range, 26.0% and 19.8%, respectively. The remaining size range percentages did not vary more than ±3% and ranged from 1.7 to 6.8%. These seven size ranges represented 24.3 to 34.2% of the total number of particles.

3.2.2. The Static Laser Heating Method

3.2.2.1. Apparatus and Procedure (Method)

In all phases of the study, the pellets were heated with a rail laser adapted to use a neodymium glass rod. Figure 3 illustrates the revised static laser heating fixture which was located in an argon atmosphere glovebox. The laser voltage was set at 2.70 keV (24-J output) with a pulse time of 5 msec. The spot diameter was 0.10 cm, and the power density calculated from the spot size was 4.0 MW/cm^2. At this power density, a temperature of 10,000 K can be expected in the vapor plume [30]. The energy input to the pellets was approximately 10,000 J/g. The laser beam passed through a 90° directional lens, a lens-prism system, and the quartz top of the static laser fixture, vaporizing a portion of the pellet. Figure 4 illustrates the complete experimental setup used for these studies. In both phases of the study, the vaporized portion of the pellet was condensed on both TEM grids and SEM stubs as shown in Figure 3.

The SEM samples were analyzed for particle size, distribution, and elements constituting the particles. The TEM samples were analyzed for particle size, shape, agglomeration (chains), and compound formation (electron diffraction).

3.2.2.2. Systems Studied and Rationale

The radioactive pellets used in the first phase of the study were composed of depleted uranium dioxide, plutonium dioxide, and reactor structural materials mixed to the following compositions (in wt %):

1) 100% UO_2

2) 100% PuO_2

3) 80% UO_2-20% PuO_2

4) 75% UO_2/PuO_2-25% 316 stainless steel

5) 75% PuO_2-25% 316 stainless steel

The depleted UO_2 was 99.5% pure. The $^{239}PuO_2$ had a plutonium assay of 0.8767 g Pu/g PuO_2 product. The isotopic analysis was 94.0% plutonium-239, 5.8% plutonium-240, 0.30% plutonium-241, and less than 0.05% plutonium-238 and plutonium-242. The 316 stainless steel was Metco 41c powder (45 to 112 μm size range). The sodium was reagent grade metal which was stored under xylene.

The materials were mixed using a mortar and pestle, charged into a 14-mm diameter graphite-coated die, and hydraulically pressed at 8.61 x 10^8 Pa in an argon atmosphere glovebox. The moisture level was less than 1.0 ppm, and the oxygen level was less than 10.0 ppm.

This study was done to provide an electron-diffraction-analysis base and an idea of the shape and size of the primary particles. In the second phase of this study, the radioactive pellet compositions were:

1) 100% PuO_2-Na (liquid)

2) 75% PuO_2-25% 316 stainless steel-Na (liquid)

3) 75% UO_2/PuO_2-25% 316 stainless steel-Na (liquid)

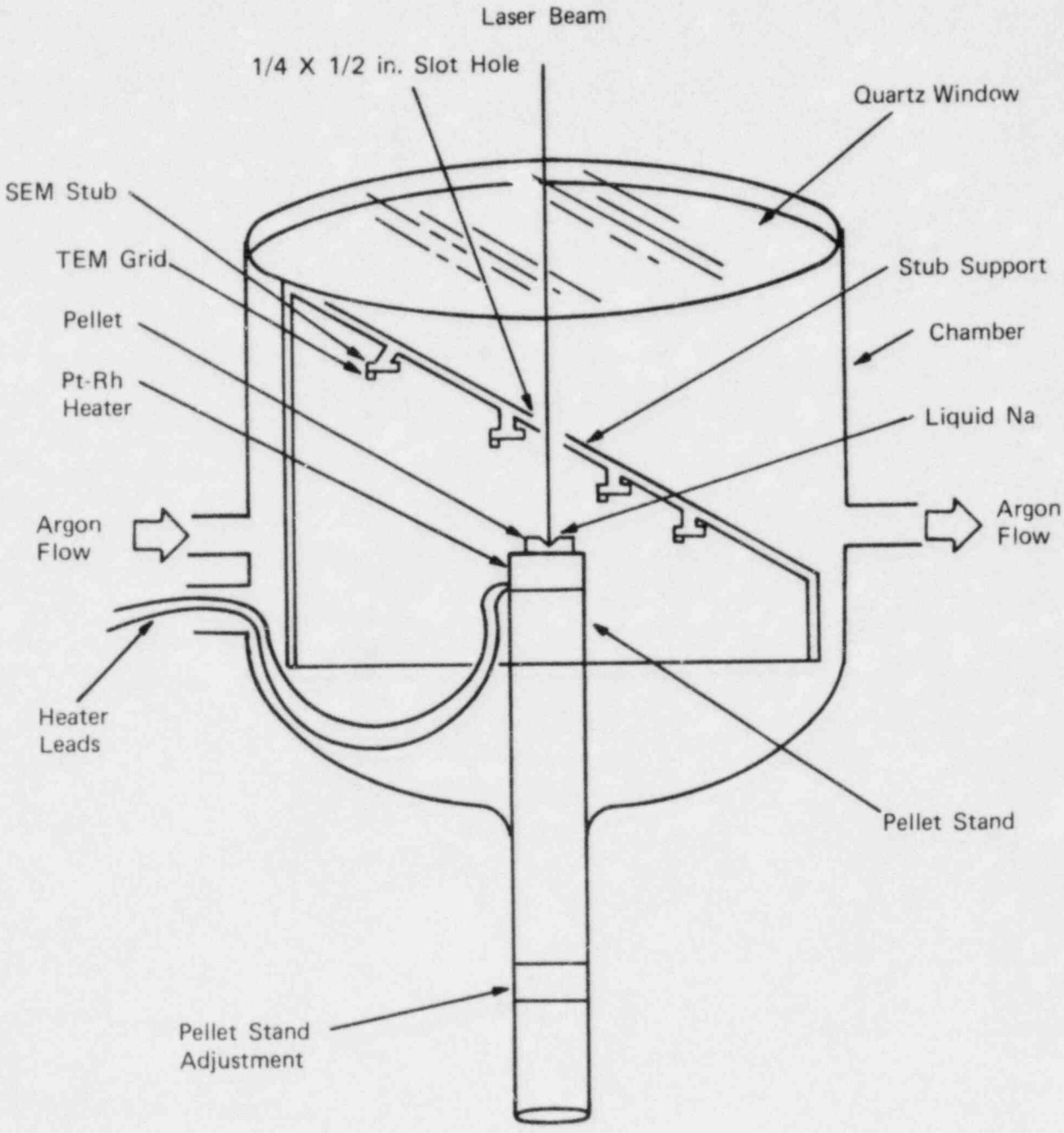

FIGURE 3 - Revised static laser heating system fixture which permits inert-gas laser heating.

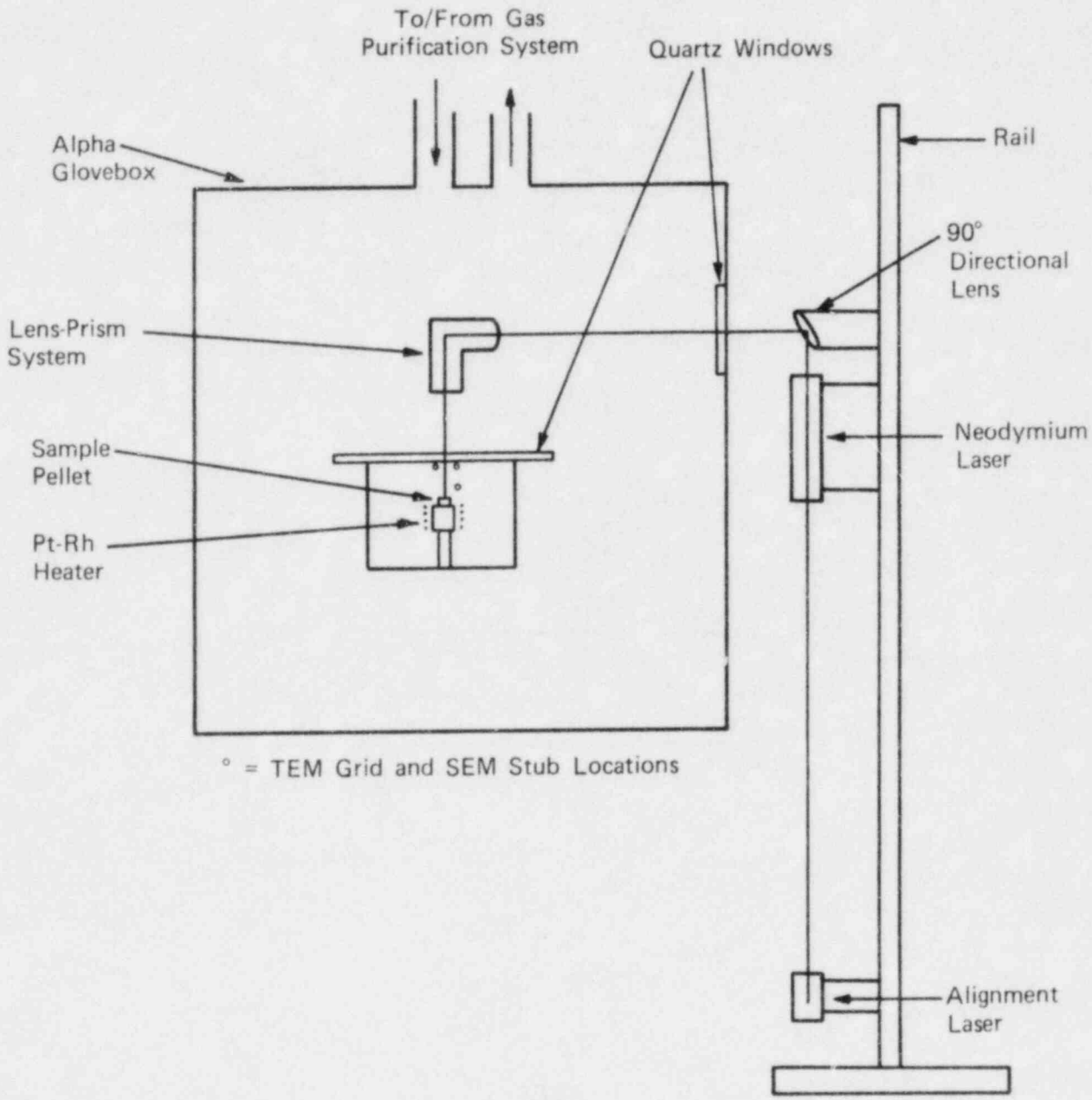

FIGURE 4 - Purified atmosphere (argon) glovebox enabling experiments with plutonium-239 and liquid sodium.

4) 75% UO_2/PuO_2-25% 316 stainless steel-Na (liquid) air

The materials used were the same as those used in the first phase of the study. The materials, after being mixed and charged into the die as described in the first phase of the study, were also pressed at 8.61×10^8 Pa in an argon atmosphere. The moisture and oxygen levels were the same as described in the first phase of the study. Sodium metal was introduced into a depression prepared in the center of the pellets. The pellets were heated to melt the sodium in the depressions just before the laser heating

This study was done to simulate the HCDA conditions in both an argon and air atmosphere. It also provided background electron diffraction analyses for the PuO_2-sodium system.

3.2.2.3. Results

Results for the two phases of the study were primarily assessed by examining the products via SEM and TEM analyses. The pellet compositions, compounds identified, and aerosol size range data collected from the TEM analyses are summarized in Tables 2 and 3.

The pellets that were laser heated without sodium formed compounds that were not different from the starting components (see Table 2). The compounds identified were UO_2, PuO_2, and FeNi. The compound FeNi is a product formed from two of the components of stainless steel, iron and nickel.

Table 2 - AEROSOL SIZES AND COMPOUNDS FORMED IN STATIC LASER EXPERIMENTS WITHOUT SODIUM

Pellet No.	System	Size (μm)	Major Compounds
1	UO_2	0.01 to 0.25	UO_2
2	PuO_2	0.01 to 0.10	PuO_2
3	80% UO_2-20%PuO_2	0.01 to 0.15	UO_2, PuO_2
4	75% UO_2/PuO_2-25% SS	0.01 to 0.25	UO_2, PuO_2, Fe
5	75% PuO_2-25% SS	0.01 to 0.25	PuO_2, FeNi

Table 3 - AEROSOL SIZES AND COMPOUNDS FORMED IN STATIC LASER EXPERIMENTS WITH SODIUM

Pellet No.	System	Size (μm)	Compounds	
			Major	Minor
1	100% PuO_2-Na (liquid)	0.01 to 0.50	PuO_2, Na_2O	Na_4PuO_5
2	75% PuO_2-25% SS-Na (liquid)	0.01 to 0.50	PuO_2, Fe, Na_2O	Na_4PuO_5
3	75% UO_2/PuO_2-25% SS-Na (liquid)	0.01 to 0.25	UO_2, PuO_2, Fe	Na_3UO_4, Na_4PuO_5
4	75% UO_2/PuO_2-25% SS-Na (liquid) (air)	0.01 to 0.15	UO_2, U_4O_9, PuO_2 Fe_2O_3, Na_2O	Na_4UO_5

The pellets that were heated with sodium formed plutonate (Na_4PuO_5) when PuO_2 was present and sodium uranate (Na_3UO_4) when UO_2 was present (see Table 3). Pellet #3 was the closest simulation to the HCDA conditions. The major products from the vaporization of the pellet were the starting components UO_2 and PuO_2, and iron a constituent of stainless steel. The minor compounds formed were sodium plutonate (Na_4PuO_5) and sodium uranate (Na_3UO_4).

Pellet #4 (Table 3) was vaporized in air to simulate the escape of the bubble from the reactor containment to the air environment of the reactor building. The major products formed were UO_2, U_4O_9, PuO_2, Na_2O, and Fe_2O_3. The minor compound formed was sodium uranate (Na_4UO_5).

An x-ray line scan of a TEM grid, that had ZrO_2 as a simulant for PuO_2, indicated that the minor compounds formed were 3 to 4% of the total composition (31). Thus, it can be concluded that the minor compounds formed with PuO_2 (Na_3PuO_4 and Na_4PuO_5) can be estimated to be 3 to 4% of the total composition, since the properties of ZrO_2 and PuO_2 are very similar.

3.2.2.4. HCDA Aerosol Formation

Figures 5, 6, and 7 are transmission electron photomicrographs of the condensation aerosols from the PuO_2, UO_2-PuO_2, UO_2/PuO_2-SS system. The particles are spherical, and the diameters range from 0.01 to 0.25 μm. The photomicrographs show branched chain-like structures that are typical of vaporization condensation aerosols of most metal oxides [30]. These branched chain-like structures from the fields of Figure 6 and 7 are shown in Figures 8 and 9.

Figures 5, 8, and 9 also show some crystalline particles that had not been observed in previous HCDA experiments [31]. The crystalline particles can be attributed to PuO_2, since they were first observed in Figure 5 and appear in systems that contain PuO_2 as shown by Figures 8 and 9. The explanation for this phenomenon is not known at this time, although it could be theorized that the lower vaporization point of PuO_2 compared to UO_2 may allow enough time during cooling for the crystalline particles to form.

Electron diffraction patterns were photographed from the particles shown in the fields of Figures 5 through 9. The compounds were discussed in the previous section and are listed in Table 2.

Figures 10 and 11 are transmission electron photomicrographs of the UO_2/PuO_2-SS-Na (liquid) system condensation aerosols. The particles are spherical, and the diameters range from 0.01 to 0.25 μm. The photomicrographs show branched chain-like structures that are slightly different from those that were vaporized without sodium. There seems to be more agglomeration of the particles, and the particles overlap more in the chain structure as can be seen in Figure 8 and 11. The particles vaporized with sodium seem to have a stronger charge than the particles vaporized without sodium, and thus the charged particles agglomerate more, causing more overlapping and compression of the chain-like structures.

Electron diffraction patterns were photographed from the particles shown in the fields of Figures 10 and 11. The compounds were discussed in the previous section and are listed in Table 3. These compounds and the spherical branched chain-like particles are expected to form as condensation products from an HCDA event.

3.2.3. Dynamic Laser Heating Method

3.2.3.1. Procedure and Apparatus (Method)

In all three phases of the study the pellets were heated with a rail laser adapted to use a neodymium glass rod. Figure 12 illustrates the dynamic laser heating fixture which was located in a nitrogen atmosphere glovebox. The laser voltage was set at 2.70 keV (40-J output) with a pulse time of 5 msec. The spot diameter was 0.10 cm, and the power density calculated from the spot size was 4.0 MW/cm^2. At this power density, a temperature of 10,000 K can be expected in the vapor plume [30]. The energy input to the pellets

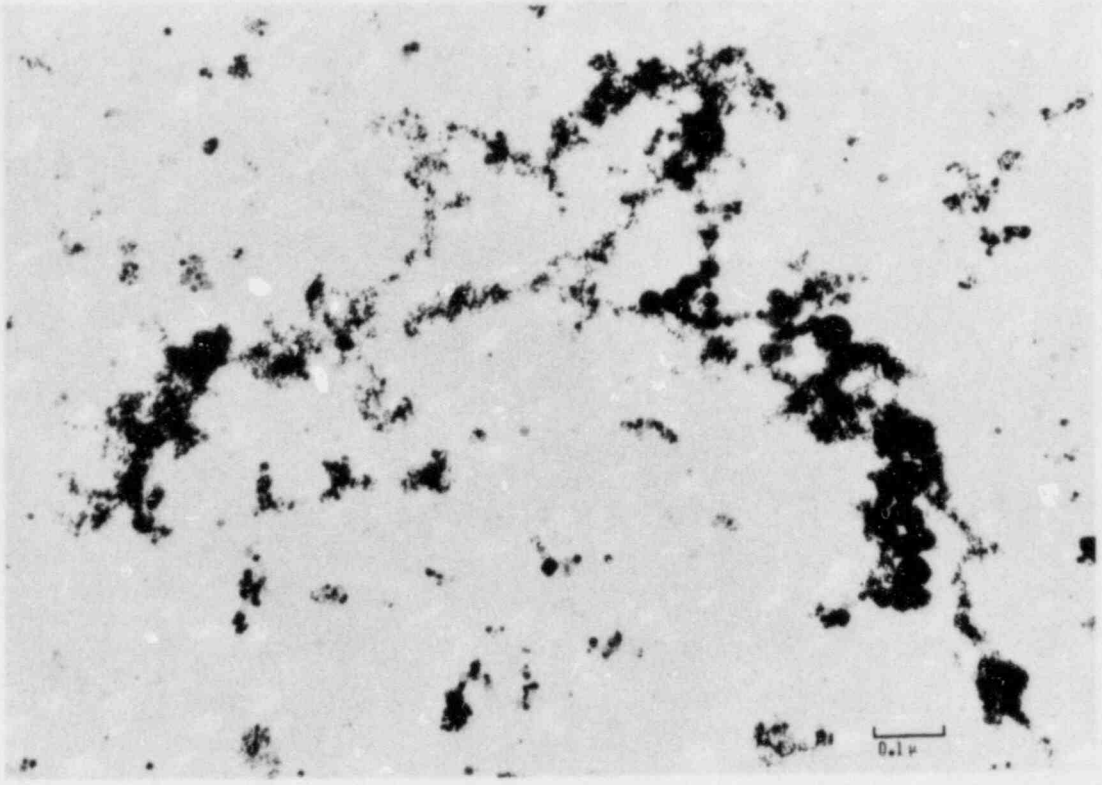

FIGURE 5 - TEM photomicrograph of laser-produced particles from a PuO_2 pellet.

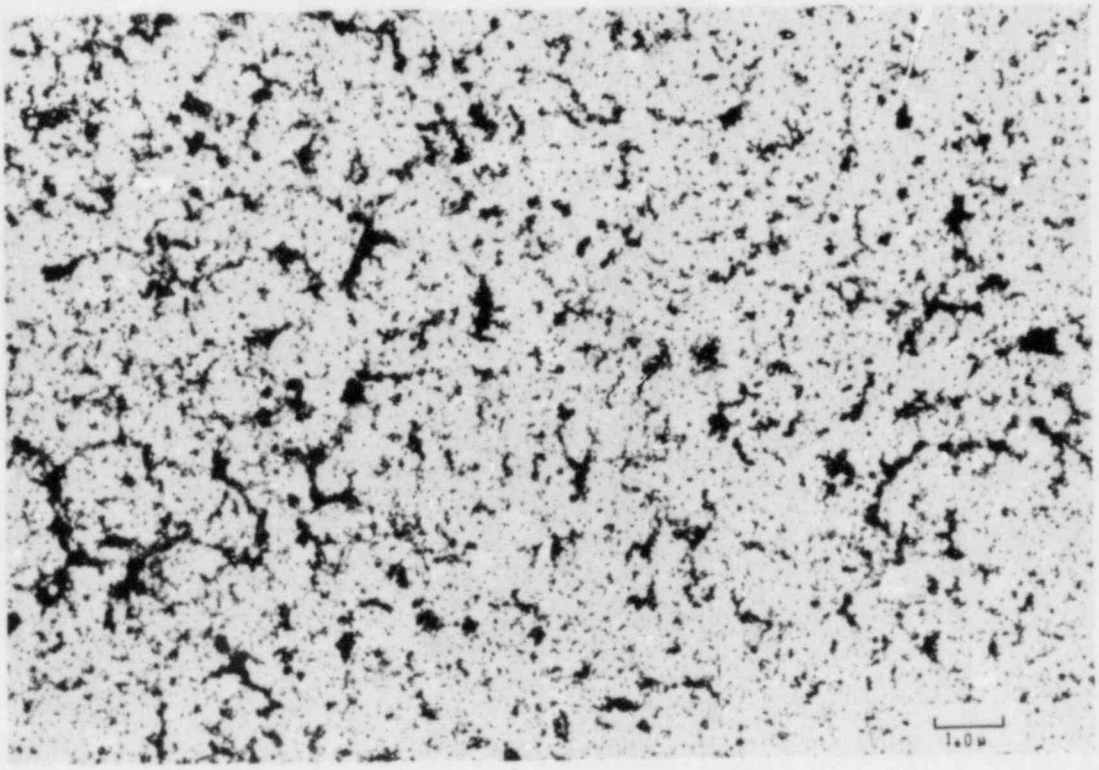

FIGURE 6 -TEM photomicrograph of laser-produced particles from an 80% UO_2-20% PuO_2 pellet.

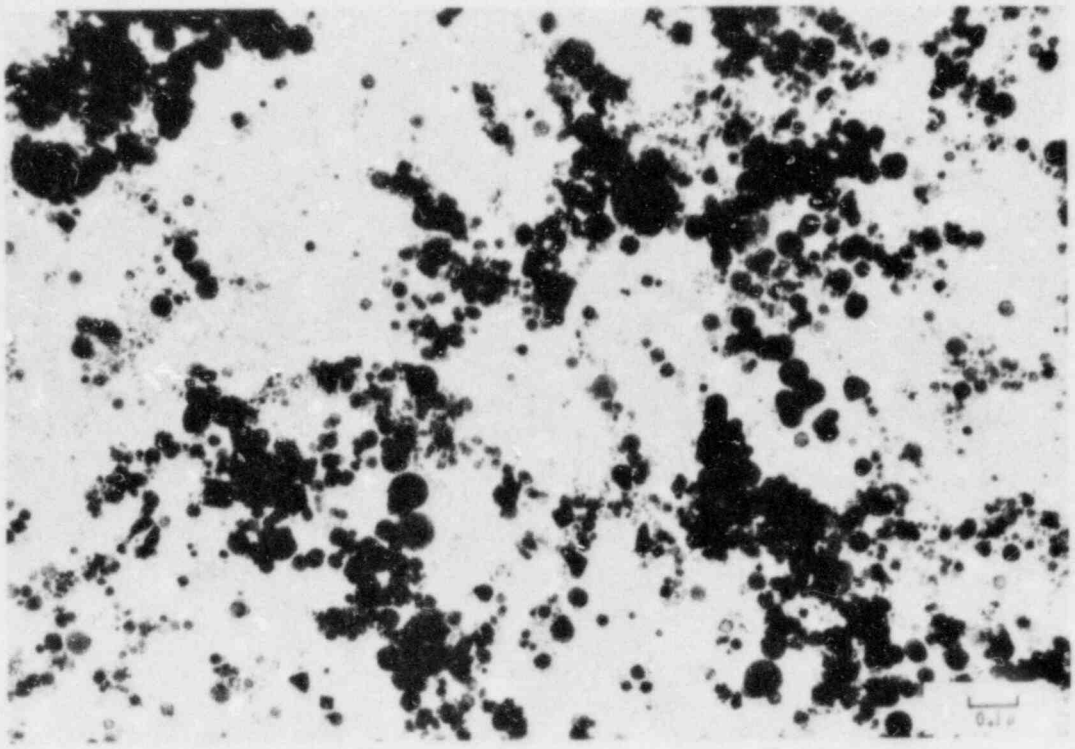

FIGURE 7 - TEM photomicrograph of laser-produced particles from a 75% UO_2/PuO_2-25% SS pellet.

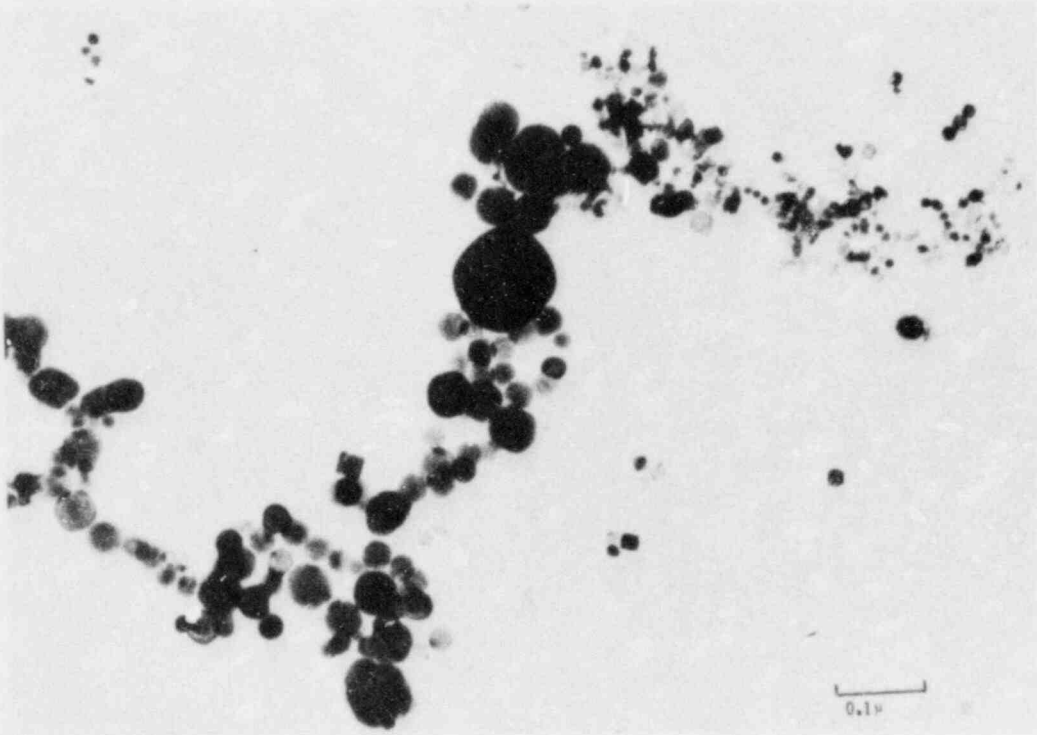

FIGURE 8 - TEM photomicrograph of laser-produced chain particles from an 80% UO_2-20% PuO_2 pellet.

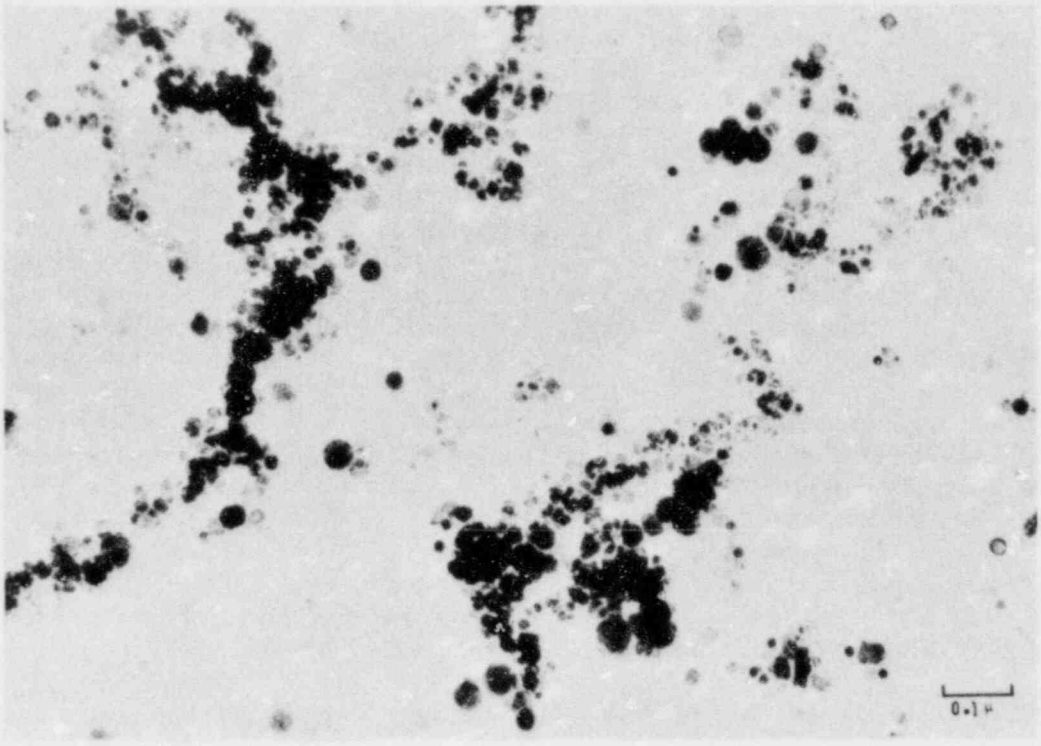

FIGURE 9 - TEM photomicrograph of laser-produced chain particles from a 75% UO_2/PuO_2-25% SS pellet.

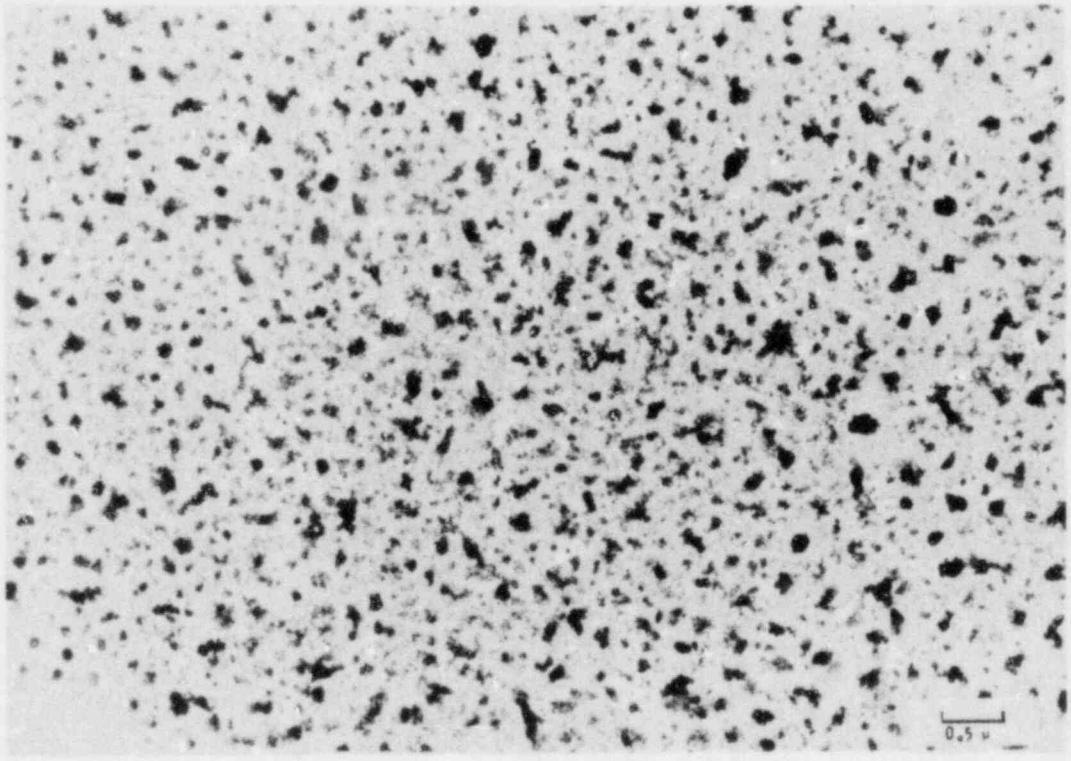

FIGURE 10 - TEM photomicrograph of laser-produced particles from a 75% UO_2/PuO_2-25% SS-Na (liquid) pellet.

was approximately 10,000 J/g. The laser beam passed through a 90° directional lens, a double mirror system, and the focusing lens of the dynamic laser fixture, vaporizing a portion of the pellet. Figure 13 illustrates the complete experimental setup used for these studies. In all phases of the study, the vaporized portion of the pellet, along with the sodium gas, is carried by an argon gas flow through the RF plasma and was condensed on both TEM grids and SEM stubs as shown in Figure 12.

The SEM samples were analyzed for particle size, distribution, and elemental constituents of the particles. The TEM samples were analyzed for particle size, shape, agglomeration (chains), and compound formation (electron diffraction).

3.2.3.2. Systems Studied and Rationale

The radioactive pellets used in the first phase of the study were composed of depleted uranium dioxide, plutonium dioxide, and reactor structural materials mixed to the following compositions (in wt %):

1) 75% UO_2/PuO_2-25% 316 stainless steel Na(gas)

The depleted UO_2 was 99.5% pure. The $^{239}PuO_2$ had a plutonium assay of 0.8767 g Pu/g PuO_2 product. The isotopic analysis was 94.0% plutonium-239, 5.8% plutonium-240, 0.30% plutonium-241, and less than 0.05% plutonium-238 and plutonium-242. The 316 stainless steel was Metco 41c powder (45 to 112 μm size range). The sodium was reagent grade metal which was stored under xylene.

The materials were mixed using a mortar and pestle, charged into a 14-mm diameter graphite-coated die, and hydraulically pressed at 8.61×10^8 Pa in an argon atmosphere glovebox. The moisture level was less than 1.0 ppm, and the oxygen level was less than 10.0 ppm.

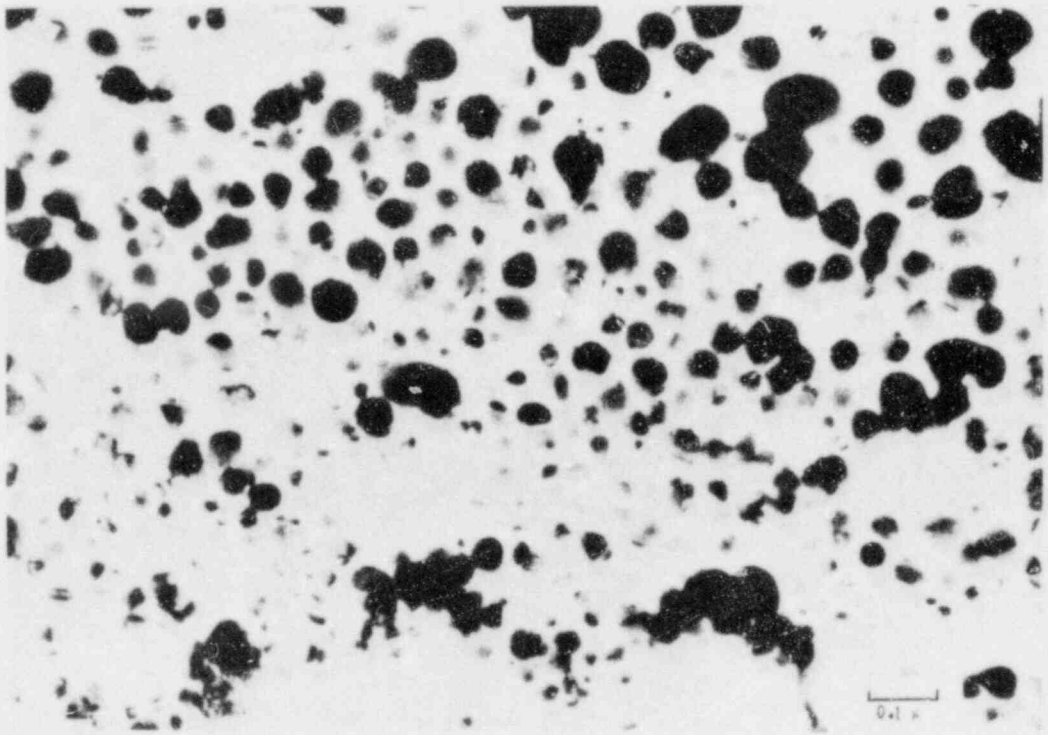

FIGURE 11 - TEM photomicrograph of laser-produced chain particles from a 75% UO_2/PuO_2-25% SS-Na (liquid) pellet.

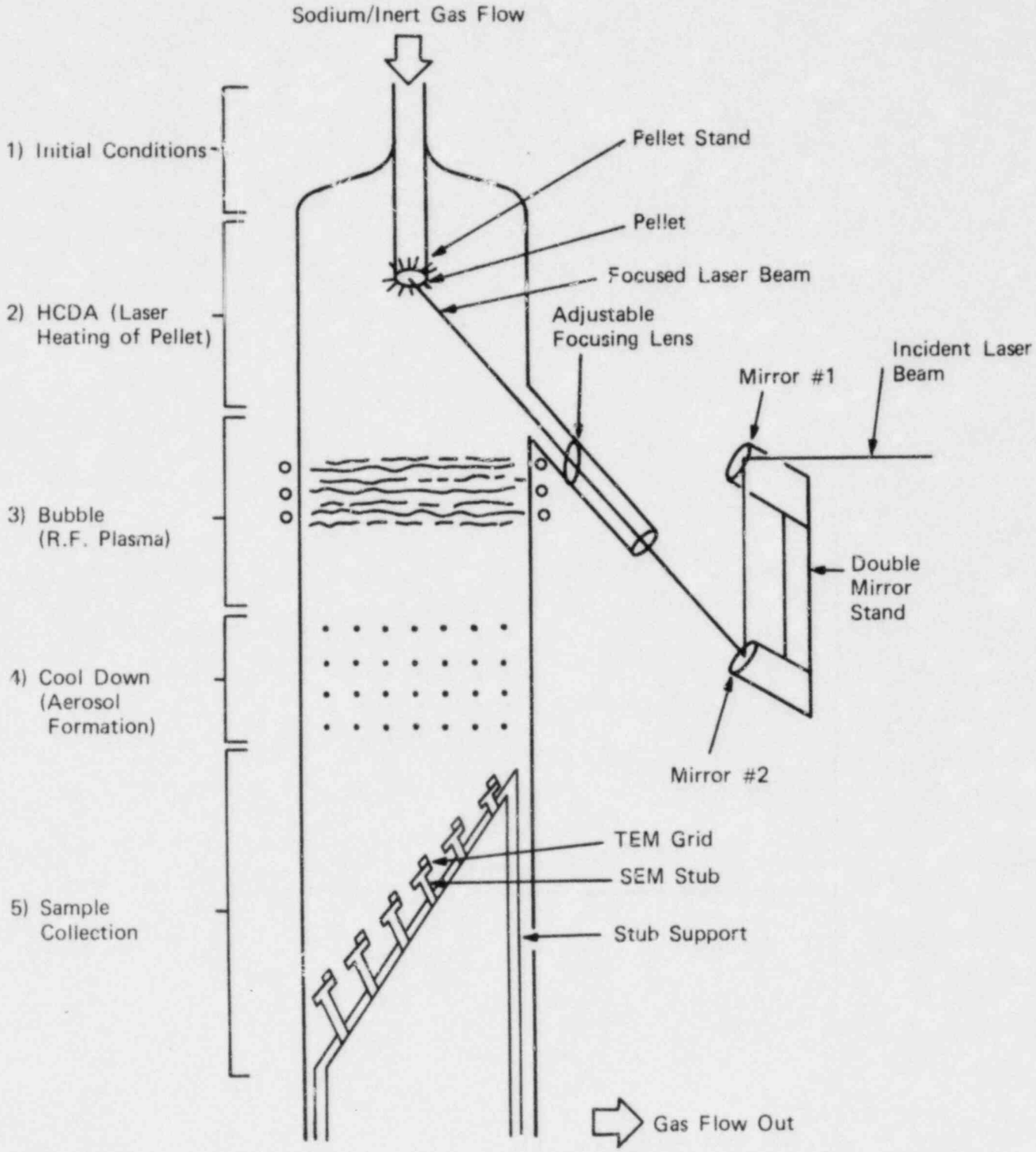

FIGURE 12 - The dynamic laser heating fixture.

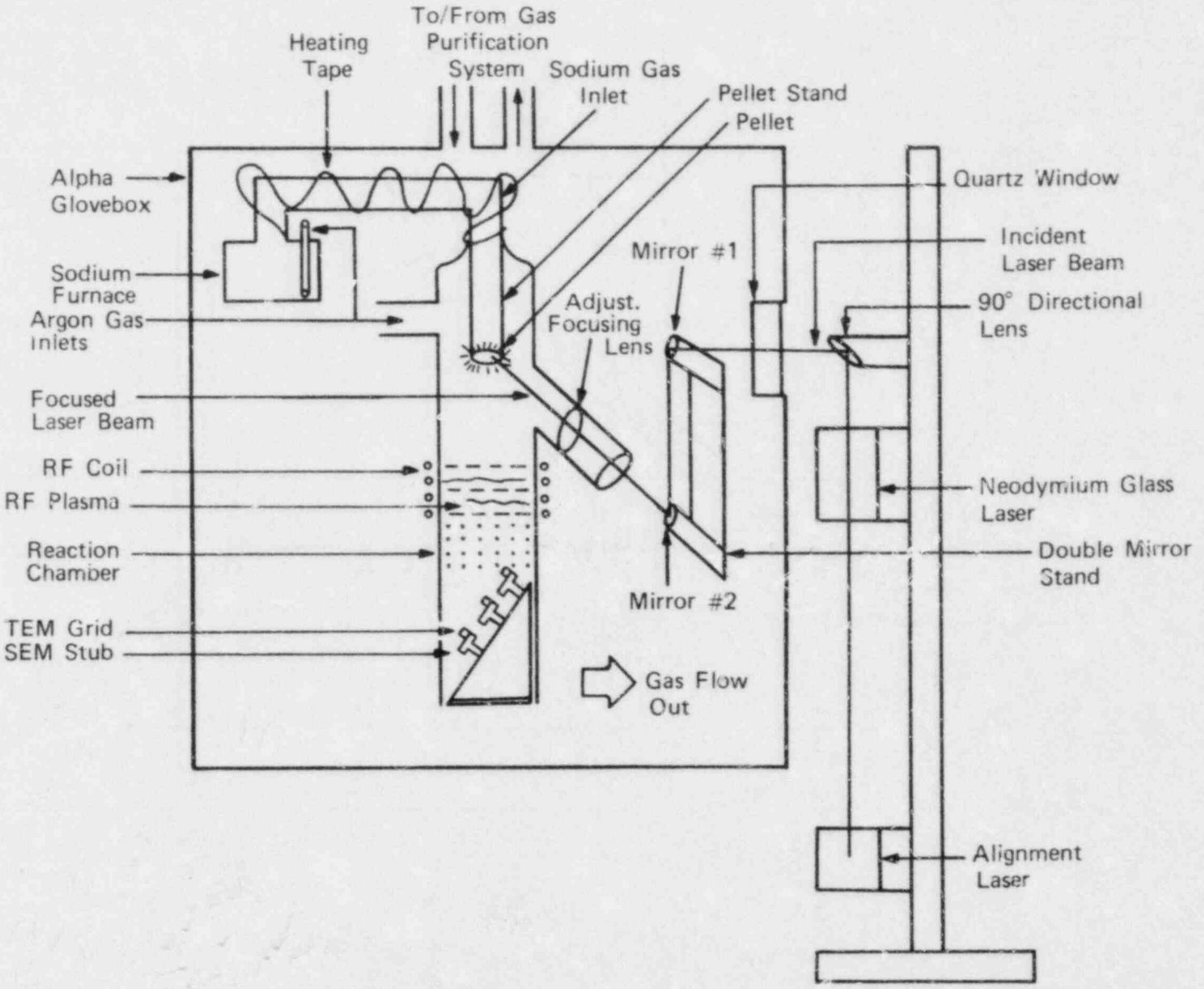

FIGURE 13 - Dynamic laser heating system.

Heated sodium gas was introduced to the pellet, and the focused laser beam was pulsed through the surrounding gas to the center of the pellet.

This study was done to compare the aerosols produced in the dynamic system with the aerosols generated in the static system.

In the second phase of the study, the radioactive pellet compositions were:

1) 80% UO_2/PuO_2-20% Te

2) 80% UO_2/PuO_2-20% BaO

3) 80% UO_2/PuO_2-20% Cs_2O

4) 90% UO_2/PuO_2-10% Te

5) 90% UO_2/PuO_2-10% BaO

6) 90% UO_2/PuO_2-10% Cs_2O

The UO_2 and PuO_2 materials were the same as those used in the first pha study. The tellurium was 99.9% pu aO was technical grade. The Cs_2O was 99.9% pure. The materials were mixed, and the pellets were pressed under the same conditions as those used in the first phase of the study. The pellets were laser heated in the same manner as the first phase of the study, except sodium gas was not used in this experiment.

This study was done to determine if there were any interactions between the UO_2/PuO_2 fuel and the fission products (Te, BaO, and Cs_2O) and to provide an electron diffraction analysis base for future, more-complicated systems.

In the third phase of the study the radioactive pellets had the following compositions:

1) 60% UO_2/PuO_2-20% 316 stainless steel-20% Te-Na(gas)

2) 60% UO_2/PuO_2-20% 316 stainless steel-20% BaO-Na(gas)

3) 60% UO_2/PuO_2-20% 316 stainless steel-20% Cs_2O-Na(gas)

4) 67.5% UO_2/PuO_2-22.5% 316 stainless steel-10% Te-Na(gas)

5) 67.5% UO_2/PuO_2-22.5% 316 stainless steel-10% BaO-Na(gas)

6) 67.5% UO_2/PuO_2-22.5% 316 stainless steel-10% Cs_2O-Na(gas)

The materials used and the method of preparation were the same as those used in the first and second phases of the study. The laser heating of the pellets and the introduction of the sodium gas were the same as those used in the first phase of the study.

This study was done to determine if there were any interactions between fuel, fission products, reactor materials, and sodium.

3.2.3.3. Results

Results for the three phases of the study were primarily assessed by examining the products via SEM and TEM analyses. The pellet compositions, compounds identified, and aerosol size range data collected from the TEM analyses are summarized in Tables 4 and 5.

The pellets that were laser heated without sodium formed compounds that were not different from the starting components (see Table 4). The compounds identified were UO_2, PuO_2, Te, BaO, Cs, and CsO_2. There was no interaction between the fuel and fission products to form a compound.

The pellets that were heated with sodium formed sodium uranate (Na_3UO_4) when UO_2 was present and $Na_3(U,Pu)O_4$ when PuO_2 was present in a mixed fuel pellet (see Table 5). Pellet #1 (Table 5) was the closest simulation to the HCDA without fission products. The major products from the vaporization of the pellet were UO_2, PuO_2, Fe, and Na. The minor compounds formed were sodium uranate (Na_3UO_4) and sodium uranium-plutonium oxide, $Na_3(U,Pu)O_4$. These results compared very closely with the results from the same composition pellet laser heated in the static system. The exceptions were Na

Table 4 - AEROSOL SIZES AND COMPOUNDS FORMED IN DYNAMIC LASER EXPERIMENTS WITHOUT SODIUM

Pellet No.	System	Size (μm)	Major Compounds
1	80% UO_2/PuO_2-20% Te	0.01 to 0.15	UO_2, PuO_2, Te
2	80% UO_2/PuO_2-20% BaO	0.01 to 0.25	UO_2, PuO_2, BaO
3	80% UO_2/PuO_2-20% Cs_2O	0.01 to 0.20	UO_2, PuO_2, CsO_2
4	90% UO_2/PuO_2-10% Te	0.01 to 0.10	UO_2, PuO_2,Te
5	90% UO_2/PuO_2-10% BaO	0.01 to 0.25	UO_2, PuO_2, BaO
6	90% UO_2/PuO_2-10% Cs_2O	0.01 to 0.15	UO_2, PuO_2, CsO_2

Table 5 - AEROSOL SIZES AND COMPOUNDS FORMED IN DYNAMIC LASER EXPERIMENTS WITH SODIUM

Pellet No.	System	Size (μm)	Compounds	
			Major	Minor
1	75% UO_2/PuO_2-25% SS-Na(g)	0.05 to 0.50	UO_2, PuO_2, Fe, Na	Na_3UO_4 $Na_3(U,Pu)O_4$
2	60% UO_2/PuO_2-20% SS-20% Te-Na(g)	0.01 to 0.25	UO_2, PuO_2, Fe, Te, Na	Na_3UO_4 $Na_3(U,Pu)O_4$
3	60% UO_2/PuO_2-20% SS-20% BaO-Na(g)	0.01 to 0.30	UO_2, PuO_2, Fe, Ba, BaO, Na	Na_3UO_4 $Na_3(U,Pu)O_4$
4	60% UO_2/PuO_2-20% SS-20% Cs_2O-Na(g)	0.01 to 0.25	UO_2, PuO_2, Fe CsO_2, Cs, Na	Na_3UO_4 $Na_3(U,Pu)O_4$
5	67.5% UO_2/PuO_2-22.5% SS-10% Te-Na(g)	0.01 to 0.50	UO_2, PuO_2, Fe, Te,Na	Na_3UO_4 $Na_3(U,Pu)O_4$
6	67.5% UO_2/PuO_2-22.5% SS-10% BaO-Na(g)	0.01 to 0.15	UO_2, PuO_2, Fe, Ba, BaO, Na	Na_3UO_4 $Na_3(U,Pu)O_4$
7	67.5% UO_2/PuO_2-22.5% SS-10% Cs_2O-Na(g)	0.01 to 0.20	UO_2, PuO_2, Fe, CsO_2, Na	Na_3UO_4 $Na_3(U,Pu)O_4$

metal, a major constituent of the dynamic system, and $Na_3(U,Pu)O_4$ formed in the dynamic system and Na_4PuO_5 formed in the static system.

3.2.3.4. HCDA Aerosol Formation

Figures 14, 15 and 16 are transmission electron photomicrographs of 80% fuel-20% fission product condensation aerosols (UO_2/PuO_2-BaO, UO_2/PuO_2-Te, and UO_2/PuO_2-Cs_2O). The particles are spherical, and the diameters range from 0.01 to 0.25 μm. The photomicrographs show branched chain-like structures that are typical of vaporization condensation aerosols of most metal oxides. These branched chain-like structures are evident in Figures 16 and 17, which show condensation aerosols from a 90% UO_2/PuO_2-10% Te system.

Figure 18 is a transmission electron photomicrograph of 75% UO_2/PuO_2-25% SS-Na(gas) system condensation aerosols. The particles are spherical and range from 0.01 to 0.50 μm. The particles compare very closely with the same composition pellet that was vaporized in the static system. Figures 11 and 18 show branched chain-like structures that are slightly different from those that were vaporized without sodium. There seems to be more agglomeration of the particles, and the particles overlap more in the chain structure as can be seen in Figures 11 and 18. The particles vaporized with sodium seem to agglomerate more, causing more overlapping and compression of the chain-like structure. Figure 19-22 are transmission electron photomicrographs of fuel-stainless steel-fission products-sodium system condensation aerosols. Figures 19 and 20 are photomicrographs of 60% UO_2/PuO_2-20% SS-20% Te-Na(gas) and 60% UO_2/PuO_2-20% SS-20% Cs_2O-Na (gas) system condensation aerosols. The particles are spherical, and diameters range from 0.01 to 0.50 μm. The photomicrographs show branched chain-like structures which are typical vaporization

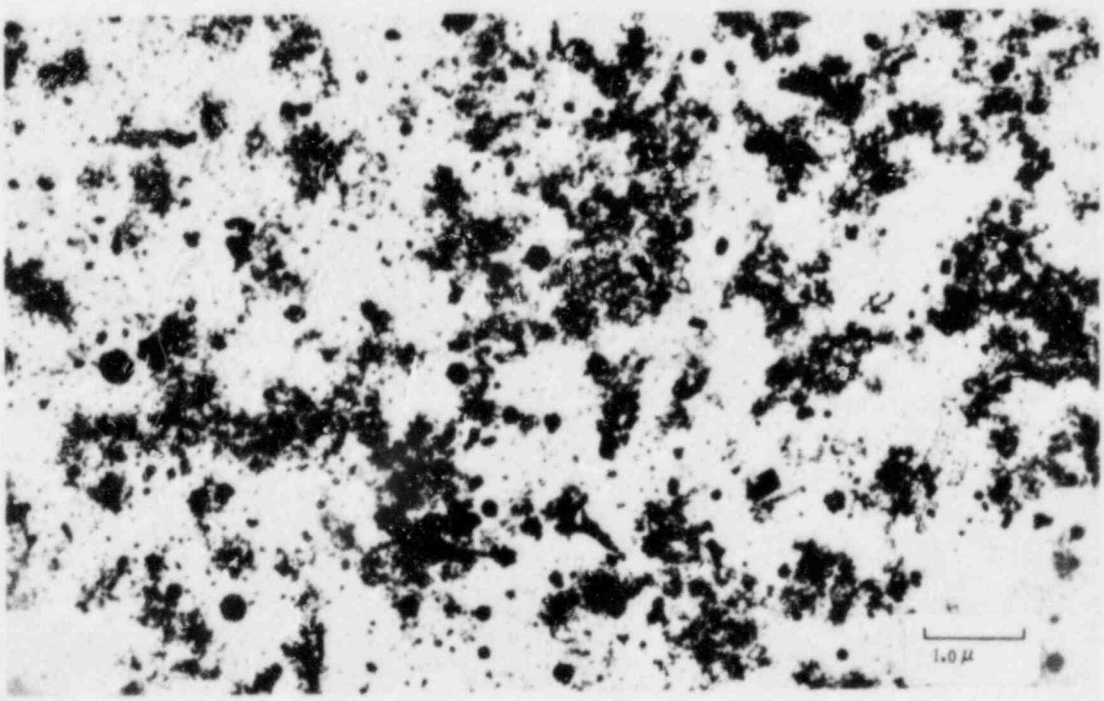

FIGURE 14 - TEM photomicrograph of laser-produced particles from an 80% UO_2/PuO_2-20% BaO pellet.

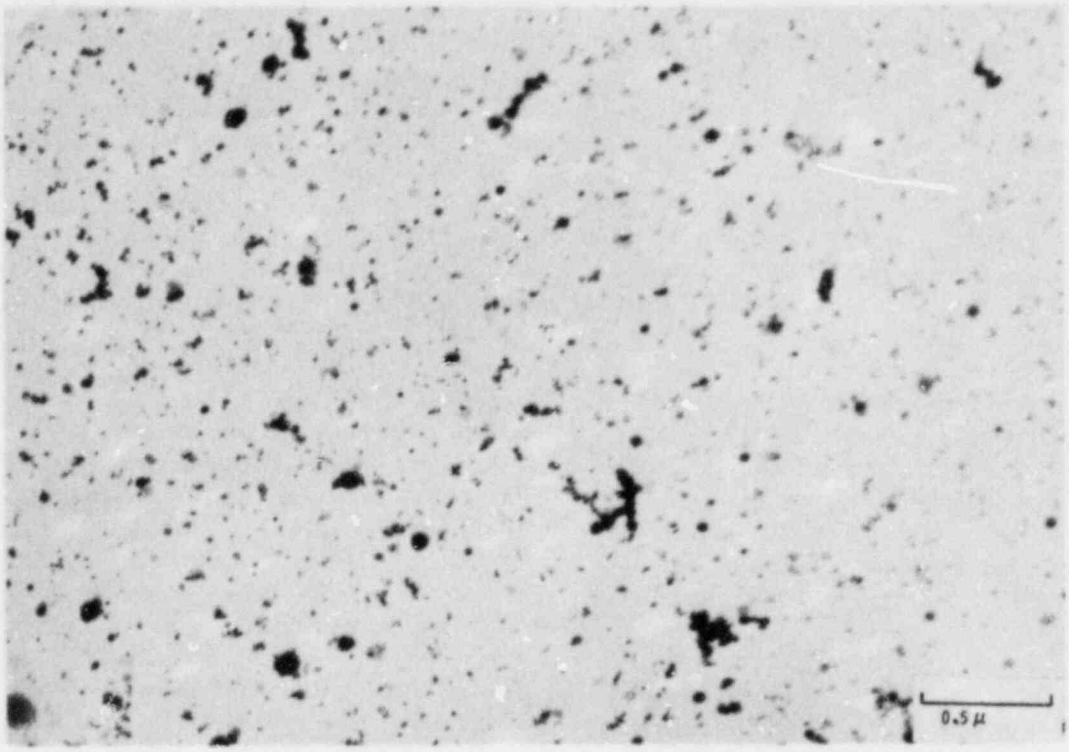

FIGURE 15 - TEM photomicrograph of laser-produced particles from an 80% UO_2/PuO_2-20% Te pellet.

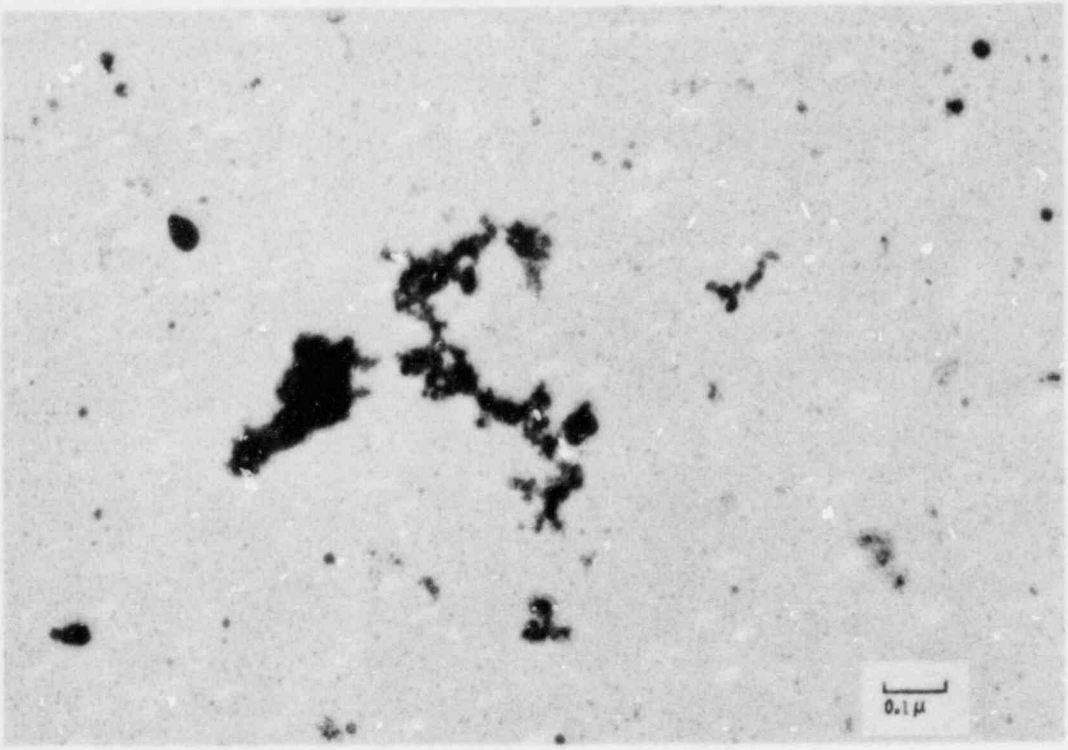

FIGURE 16 - TEM photomicrograph of laser-produced chain particles from an 80% UO_2/PuO_2-20% Cs_2O pellet.

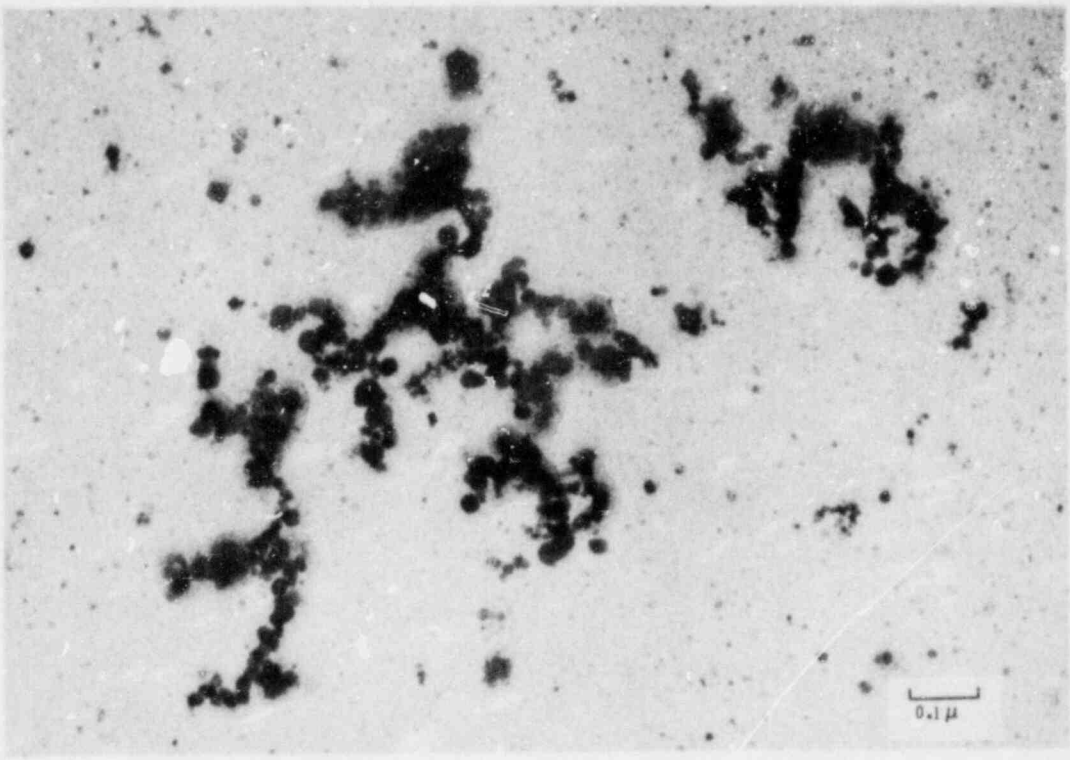

FIGURE 17 - TEM photomicrograph of laser-produced chain particles from a 90% UO_2/PuO_2-10% Te pellet.

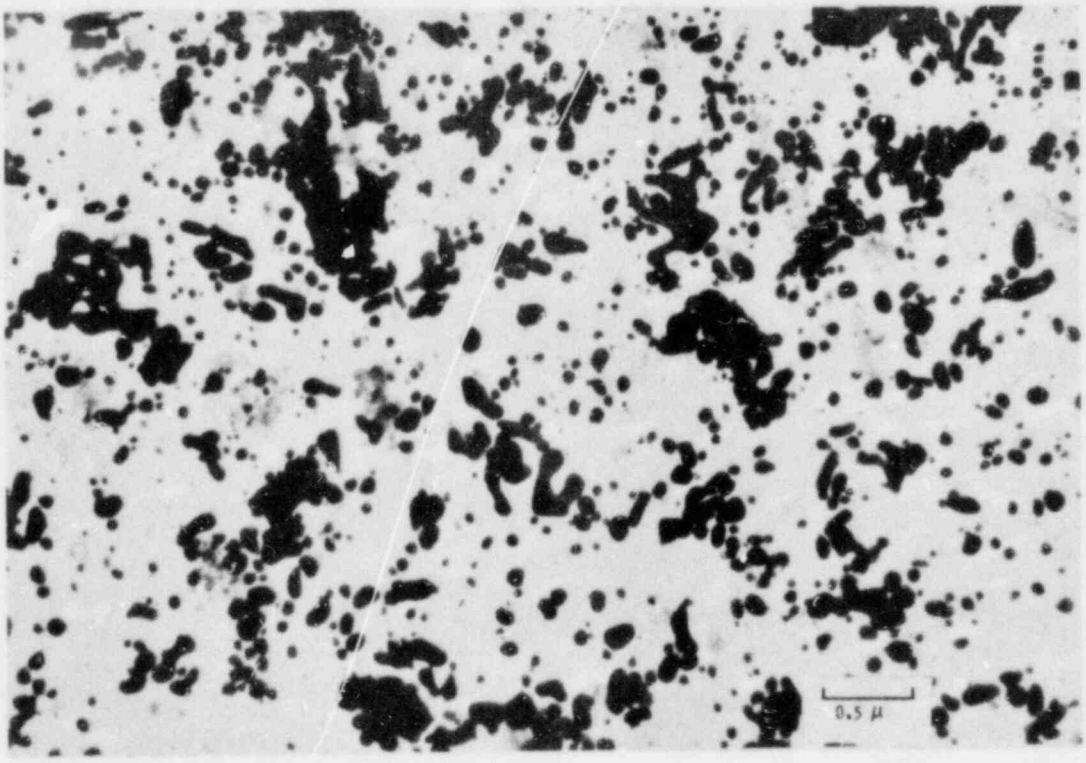

FIGURE 18 - TEM photomicrograph of laser-produced chain particles from a 75% UO_2/PuO_2-25% SS pellet and Na(g).

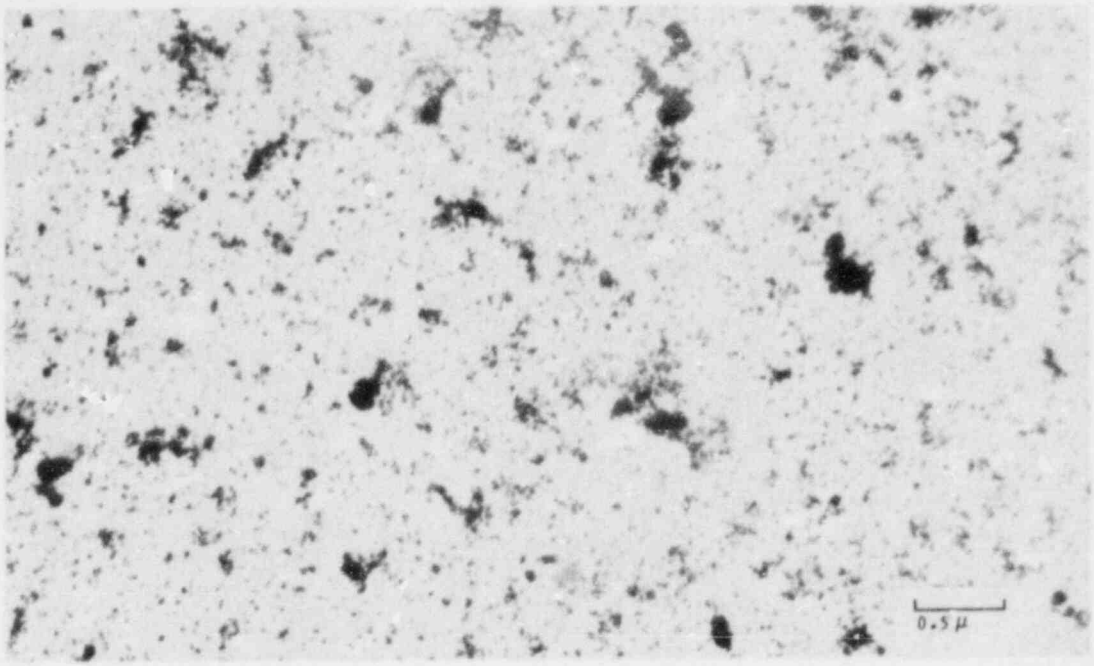

FIGURE 19 - TEM photomicrograph of laser-produced particles from a 60% UO_2/PuO_2-20% SS-20% Te pellet and Na(g).

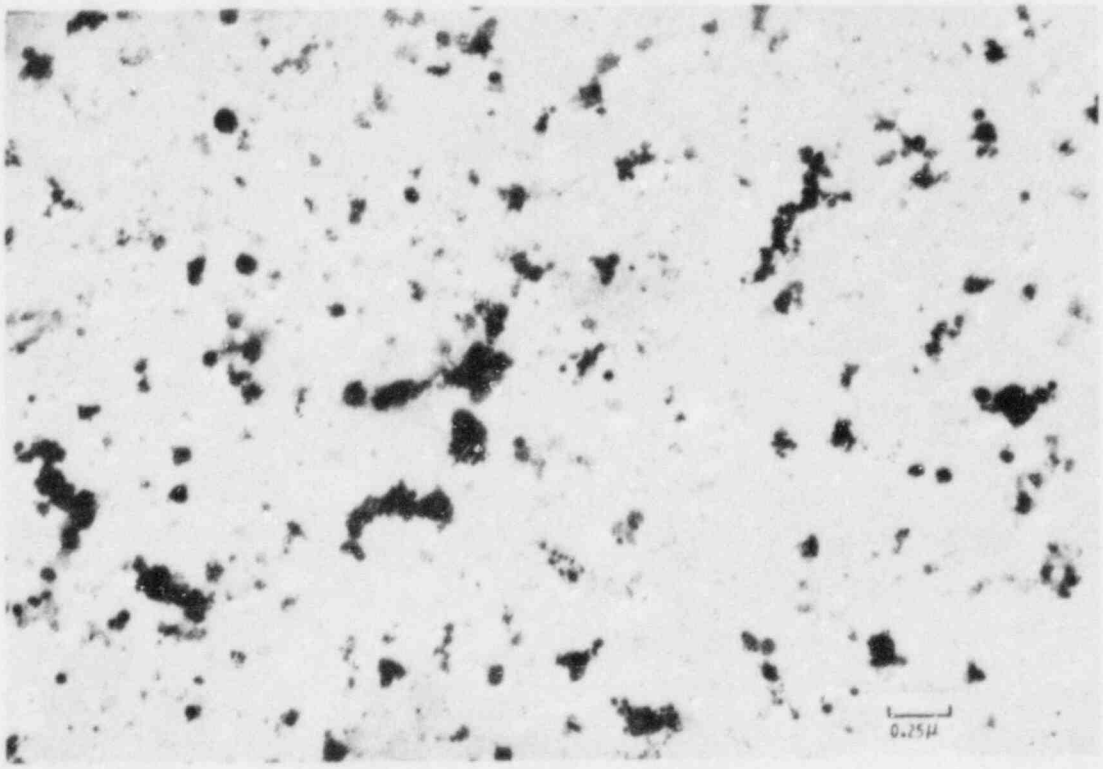

FIGURE 20 - TEM photomicrograph of laser-produced particles from a 60% UO_2/PuO_2-20% SS-20% Cs_2O pellet and Na(g).

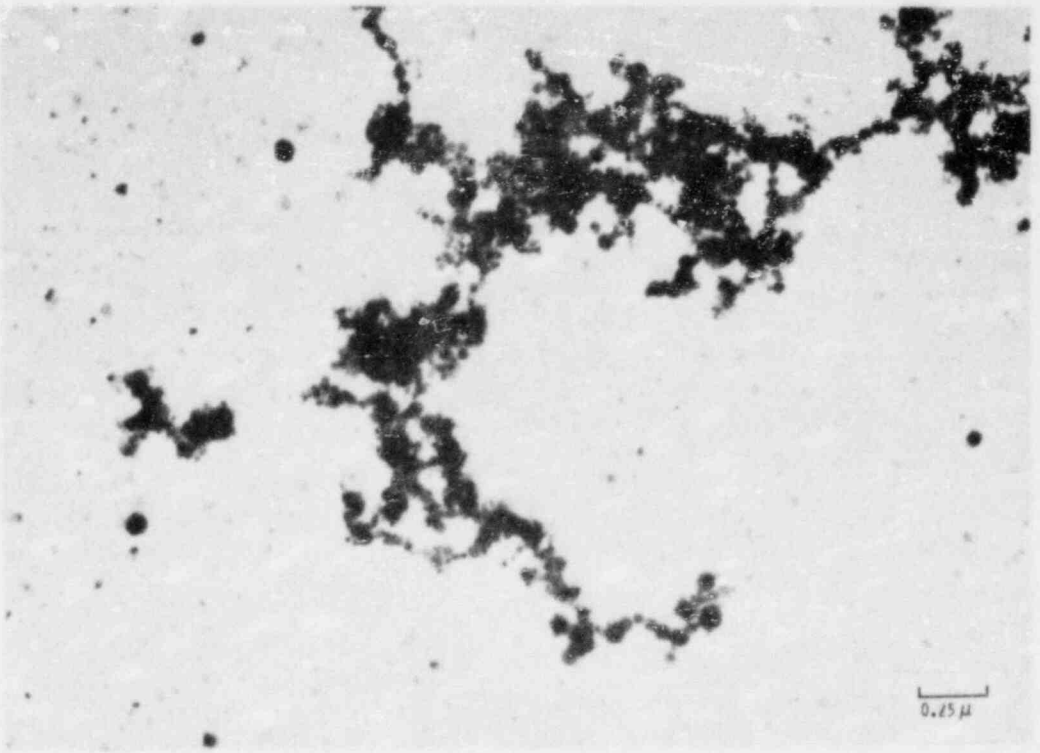

FIGURE 21 - TEM photomicrograph of laser-produced chain particles from a 67.5% UO_2/PuO_2-22.5% SS-10% Te pellet and Na(g).

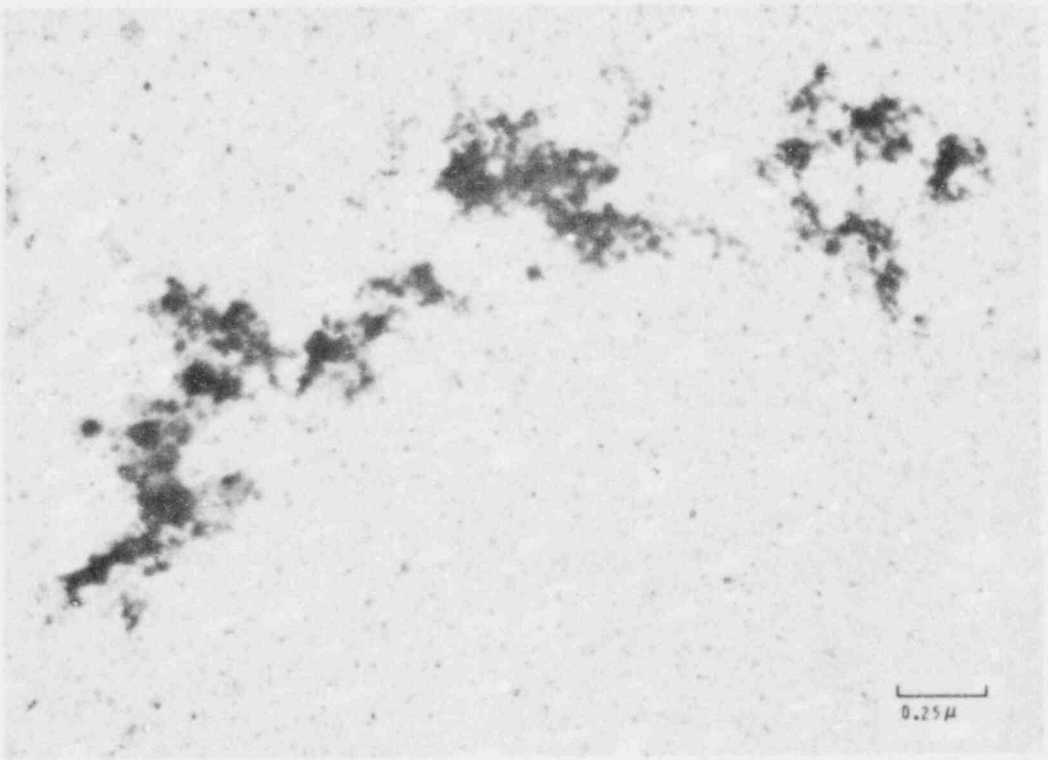

FIGURE 22 - TEM photomicrograph of laser-produced chain particles from a 67.5% UO_2/PuO_2-22.5% SS-10% BaO pellet and Na(g).

condensation aerosols of most metal oxides. Figures 21 and 22 are photomicrographs of these chain-like structures from the 67.5% UO_2/PuO_2-22.5% SS-10% Te-Na(gas) and 67.5% UO_2/PuO_2-22.5% SS-10% BaO-Na(gas) system condensation aerosol. The chain-like structures show the agglomeration and compression effect that seems to be typical of condensation aerosols in the presence of sodium.

Although the effect does not seem to be as great when fission products are present, the effect was evident on all aerosols that were generated with sodium present. The compounds in Tables 4 and 5 are expected to form in spherical branched chain aerosols during condensation from an HCDA event.

3.3. DISCUSSION

3.3.1 Comparison of the Simulation Methods

The capacitance discharge unit (CDU) method did not simulate the HCDA conditions as well as the static and dynamic laser evaporation methods. This was evident from the compounds identified and from the particle size analyses. The compounds generated were various forms of the starting materials. No interactions of sodium with uranium to form sodium uranates were evident, as was the case when the laser evaporation method was used.

The particle sizes that were produced by the CDU method ranged from <5 to 50 μm compared to very small (0.01 to 0.50 μm) particles that were produced by the laser evaporation method. Several reasons have been proposed as to why the difference existed. The main reason proposed was that the UO_2 was not vaporized but reached only a white hot liquid state as verified by high speed photography [32]. This liquid state was not as conducive to interaction of the sodium and UO_2 to form sodium uranates as the gaseous state, as evidence by the laser evaporation methods. This liquid state was also conducive to larger particles being formed. The vaporization of UO_2 produces small branched chained-like structures (0.01 to 0.50 μm) that are typical of vaporization condensation aerosols of most metal oxides [30]. This was evident from the laser evaporation methods. Since the laser evaporation methods produced the expected aerosols, and the CDU method was not vaporizing the metal oxides, the CDU method was abandoned for the more rewarding laser evaporation methods.

The laser evaporation methods, static and dynamic, compared very closely with each other and very closely with the literature. The range of particle sizes for both systems was 0.01 to 0.50 μm, which compared with predicted values of 0.1 to 0.38 μm [19]. In both methods the branched chain-like particles were typical, and most of the particles were spherical. Some cubic particles were also noted in both methods. When sodium was present, the particles were slightly larger, and the chain-like structures agglomerated or became more compressed. This was evident in both methods.

The compound formation from the starting material compared very closely in both methods. The compounds from the fuel (UO_2,PuO_2), stainless steel (Fe,Ni), sodium (Na,Na_2O), and fission products (Te, Cs_2O, BaO), which were starting components, were also the typical compounds formed in both methods. The compound formation from the interaction of fuel and fission products with sodium were different in each method, with the exception of the sodium uranate compound Na_2UO_4. Na_2UO_4 was formed in both methods. In the static laser evaporation method, the sodium plutonate compound Na_4PuO_5 was formed. In the dynamic laser evaporation method, the sodium mixed-oxide plutonate compound $Na_3(U,Pu)O_4$ was formed.

The advantage of the dynamic laser system over the static laser system is that the dynamic laser heating method simulates the HCDA scenario more closely by providing a longer high-temperature residence time. Thus, the results from the dynamic laser heating method are more representative of the HCDA conditions than the results from the static laser heating method.

3.3.2 Theoretical considerations

3.3.2.1 Thermodynamics

The standard free energy changes for the reactions of the following general equation have been calculated for all systems on which sufficient thermochemical data exist [31]:

$$xNa(g) + yU(g) + zO(g) \rightarrow Na_xU_yO_z(c) \quad (1)$$

The results of the calculations are shown in Figure 23. The thermochemical data upon which the calculations are based are in most cases considered accurate up to about 3000 K. Because of the near linearity of the curves, it is reasonable to extend the calculations to about 5000 K. Above this temperature the validity of further extension is questionable because of the increasing importance of electronically excited states that when accessible, add large amounts to the heat capacity of a species. Inspection of Figure 23 shows that at temperatures above about 5000 K $UO_2(c)$ is more stable than are any of the sodium uranates except $Na_2UO_4(c)$, while at temperatures below about 3000 K, $UO_2(c)$ is less stable than are any of the sodium uranates. If equilibration is allowed between all possible products, then $Na_2U_2O_7(c)$ would be the expected product at low temperatures. This, of course, is not what is observed. The reason is that equilibration between all the products is not possible because of prohibitively high kinetic barriers.

An alternate approach to predicting the major product from Figure 23 is to consider a process beginning at a temperature in excess of 5000 K and to simulate a cool-down process by following the temperature axis to the left. For the present, ignore $Na_2UO_4(c)$. As one looks at a cool-down, it may be noted that the first product to become stable is $UO_2(c)$. The next is $NaUO_3(c)$. By this time, however, $UO_2(c)$ formation is more stable by about 50 kcal/mole. Because of the essentially irreversible nature generally observed in solid formation, it is felt that the first product to begin to seed out [here $UO_2(c)$] will be the major product because its formation will use up all the reactants before the system cools enough to allow other possible products to become stable. $Na_2UO_4(c)$ is an anomaly in this analysis; thermodynamically it should be the first product to seed out. Evidently a kinetic barrier prevents this. This disagreement between the experiment and the thermodynamic prediction illustrates the need for kinetic studies of the HCDA.

There is experimental evidence that there can be equilibration between some (but not all) of the possible products in an HCDA. Specifically, Blackburn has studied the equilibrium [33]

$$UO_{2(c)} + 3Na_{(l)} + O_{2(g)} \rightleftharpoons Na_3UO_{4(c)} \quad (2)$$

at 900 °C. His work shows that $Na_3UO_{4(c)}$ formation can be favored if excess oxygen is available either as dissolved gas or nonstoichiometric oxygen-rich uranium oxide. Rough kinetic data from Blackburn's work show that essentially all the $UO_{2(c)}$ formed in the simulated HCDA could be converted to $Na_3UO_{4(c)}$ in 1 msec. We conclude that Na_2UO_4 is the thermodynamically favored product at high temperatures. The reason it is not observed experimentally is that its formation is prohibited by chemical kinetics. The next product to "seed out" according to the thermochemical analysis is $UO_{2(c)}$. As the cool-down continues to about 1200 K, the reaction of Equation 2 explains the experimental observation of $Na_3UO_{4(c)}$ in addition to $UO_{2(c)}$.

3.3.2.2 Kinetics

The sodium-mixed uranium/plutonium oxide reaction is represented by

$$3x\ Na_{(g\ or\ l)} + (1+x)MO_{2(s)} \rightarrow xNa_3MO_{4(s)} + MO_{2-2x(s)} \quad (3)$$

with M = U + Pu in the ratio Pu/(U+Pu) = 0.20. In the best experimental work presently available on the kinetics of this reaction, the volume change of the mixed oxide pellet was followed as a function of time at three temperatures, 700, 800, and 900 °C [34]. Because the volume change is related to the

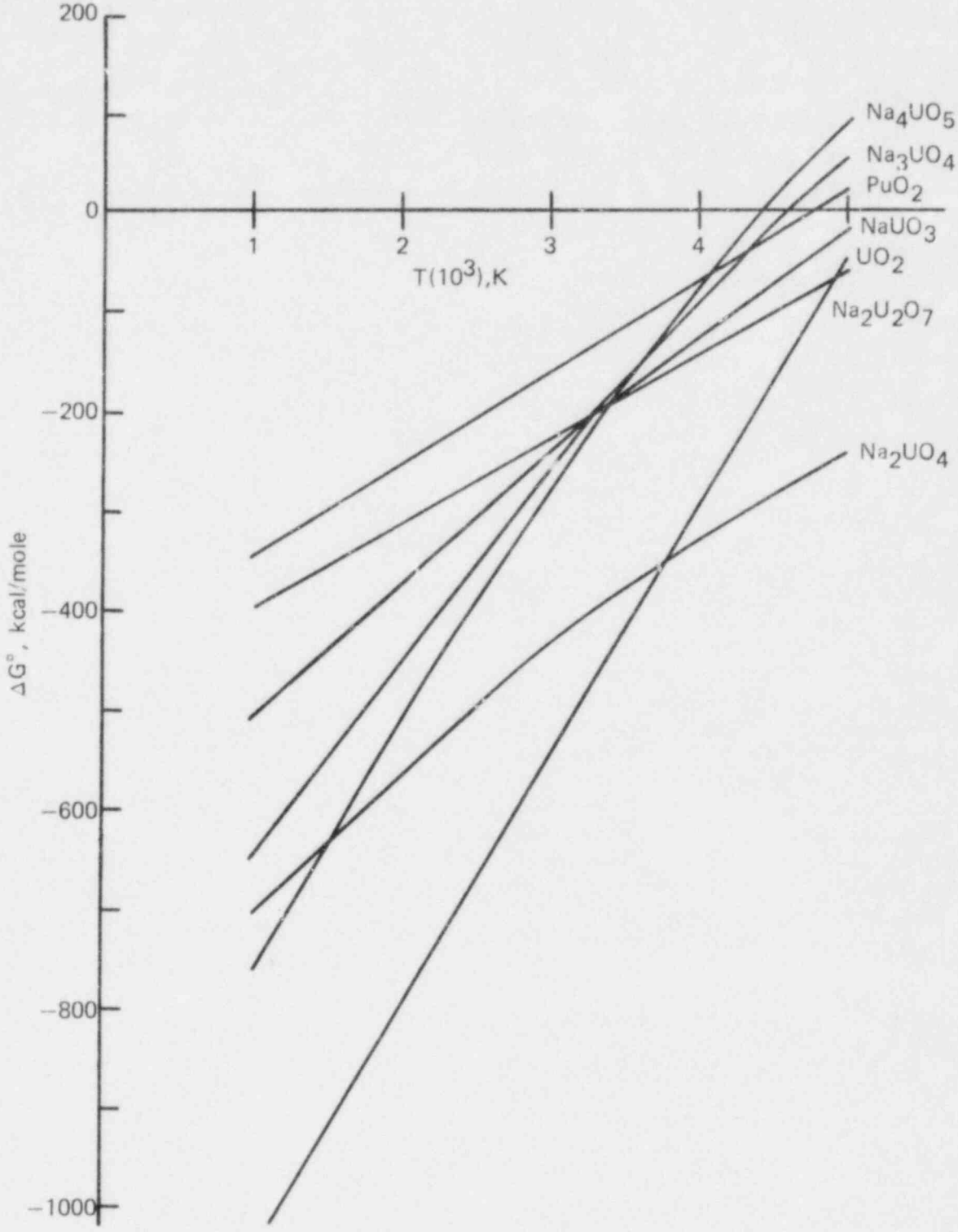

FIGURE 23 - Behavior of free-energy change as a function of temperature calculated for various potential products.

reaction extent, Martin's data contained sufficient information to allow a temperature-dependent rate law for Reaction 3 to be extracted. This section of this report discusses how the rate law was extracted, its implications, its limitations, and methods for determining a more reliable rate law.

The theoretical maximum increase in the volume of the mixed-oxide pellet after completion of reaction is 4.44%. The time data confirm this theoretical value [34]. Some pellets were observed to expand more than 4.44%, but these observations could be explained by cracks and fissures found in pellets. The reaction extent, α, may then be taken to be the observed volume expansion divided by its theoretical maximum value.

The next step in the analysis was to find a rate law based on a physical reaction model which fits the data. Three integral rate laws were examined. Using a first order rate law,

$$\ln(1-\alpha) = -kt, \tag{4}$$

where k is the rate constant and t is the time, the fit of the data to a linear function of t was poor. In addition, there was no physical basis for using a first order rate equation for the reaction of interest here. Second, using the equation:

$$-\ln(1-\alpha) = kt^3 \tag{5}$$

which corresponds physically to the growth of spherical nuclei, the fit of the data was very poor. This law would apply if the reaction involved a gas-solid interaction at the pellet surface. Finally, the expression,

$$1-(1-\alpha)^{1/3} = kt \tag{6}$$

which corresponds physically to movement of a spherical phase boundary, was tried [35]. This rate law seems most plausible for a liquid-solid reaction at the pellet surface. When the data at 700 °C were plotted (see Figure 24) using Equation 6, a straight line was obtained except in the region representing the last stages of reaction where deviation might be expected because of side reactions and possible sublimation. At 800 and 900 °C, the fit (see Figure 25) is hard to evaluate because most of the data points were taken after the major part of the reaction had already occurred. The experiments at 800 and 900 °C should be repeated with measurements made at much shorter intervals so that the early stages of reaction can be observed.

The rate constants were determined at 700, 800, and 900 °C from the slopes of the best fit lines. The values are poor at 800 and 900 °C for the reasons discussed above. Table 6 shows the rate constants extracted at each temperature. Using Arrhenius analysis, the data in Table 6 were fitted to a straight line according to the linear least squares method, which gave a coefficient of determination, r^2 (measure of goodness of fit), of 0.899. From the coefficients a temperature-dependent rate constant,

$$k = 10^{16.88} \exp(-40{,}272/T) \tag{7}$$

could be written, the kinetic parameters of which are:

$E_a = 80.0$ kcal-mol^{-1} and $A = 10^{16.88}$ day^{-1} or

$A = 8.8 \times 10^{-11}$ sec^{-1}.

From Equations 6 and 7, the time for 90% completion of reaction, $t_{0.9}$ was easily obtained as:

$$t_{0.9} = \frac{0.54}{10^{16.88} \exp(-40{,}272/T)} \tag{8}$$

where $t_{0.9}$ is in days. From Equation 8, reaction times were calculated for several temperatures of interest: 5000 K, 3100 K (inside bubble temperature), and 1200 K (outside bubble temperature). These times are shown in Table 7.

Inspection of Table 7 shows that at the temperature of the inner part of the bubble, the reaction can proceed essentially to completion in less than a microsecond. The formation and subsequent observation of Na_3MO_4 is, therefore, explicable from the kinetic data.

The rate constant in Equation 7 may be in considerable error for several reasons. First, as mentioned previously, the data at 800 and

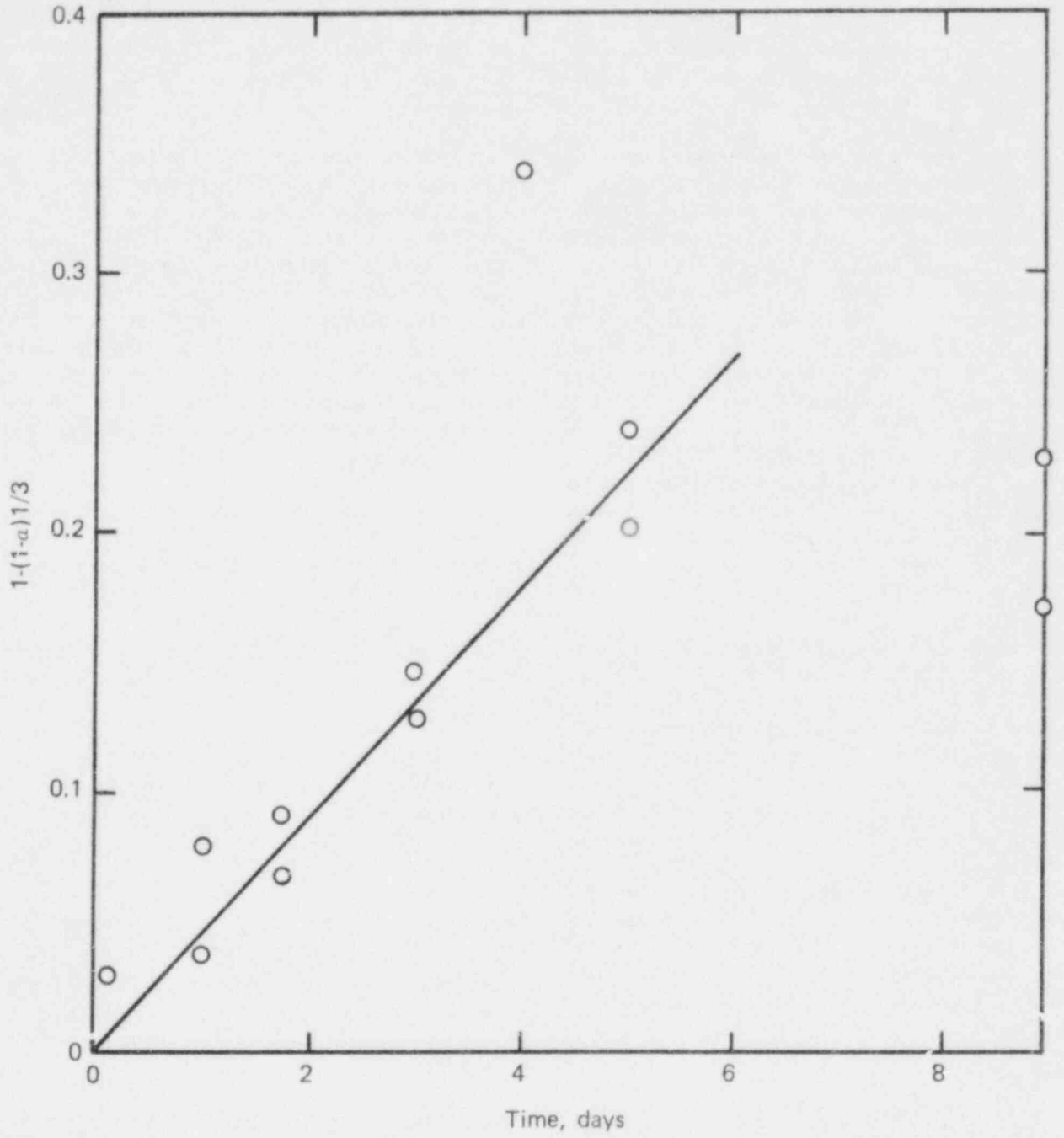

FIGURE 24 - Three-dimensional phase boundary movement at 700 °C yielded a straight line except in the last stages of reaction.

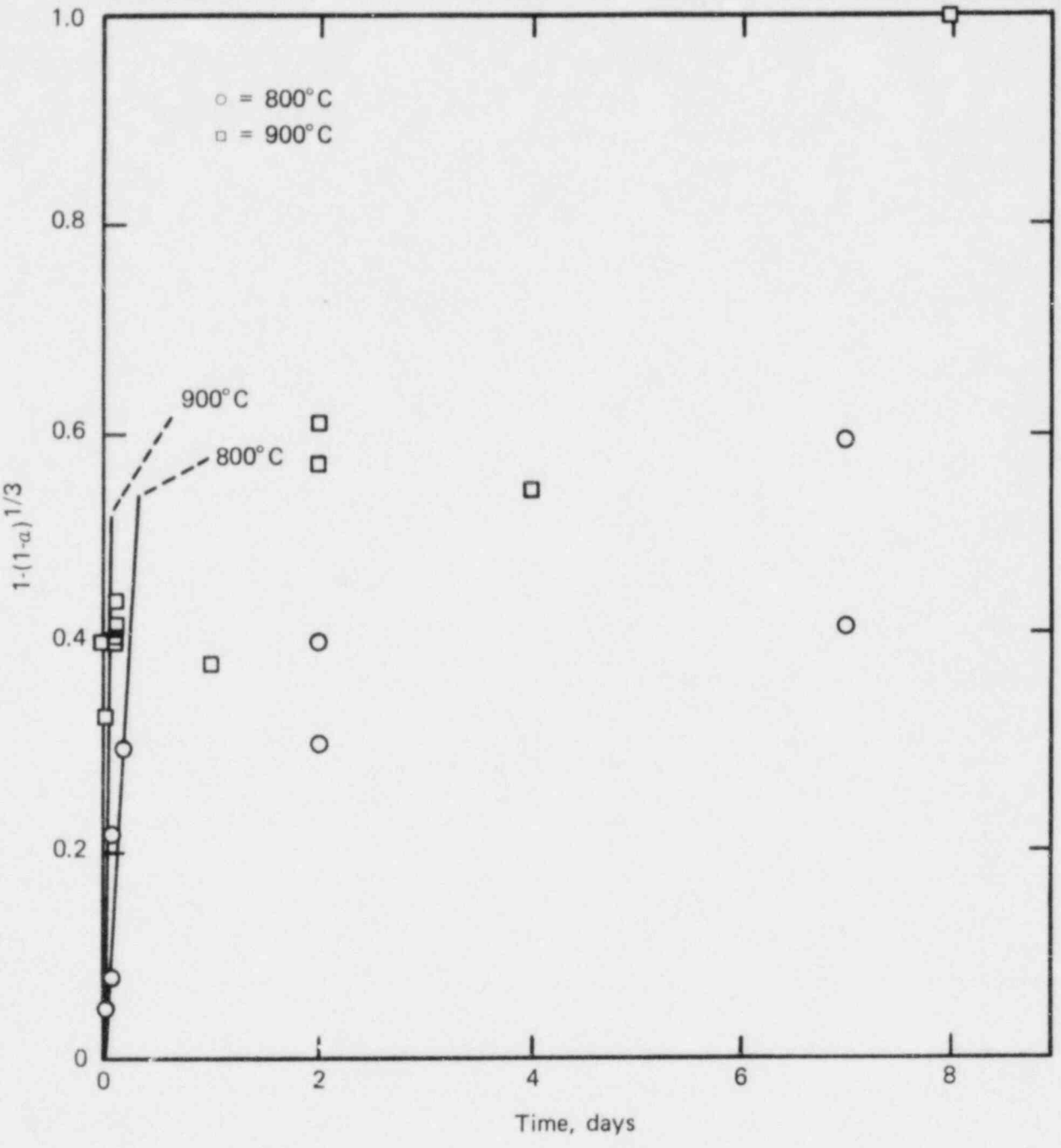

FIGURE 25 - Three-dimensional phase boundary movement at 800 and 900 °C was difficult to evaluate with the present data.

Table 6 - THE RATE CONSTANT, k, FOR SODIUM-MIXED OXIDE REACTIONS WAS DETERMINED FROM THE DATA PLOTTED IN FIGURES 24 AND 25

Temperature (°C)	Temperature (K)	$1/T(K^{-1})$	$k(day^{-1})$	ln k
700	973	10.277×10^{-4}	4.40×10^{-2}	3.12
800	1073	9.320×10^{-4}	15.0	2.71
900	1173	8.525×10^{-4}	45.0	3.81

Table 7 - THE TIME REQUIRED FOR COMPLETION OF SODIUM-MIXED OXIDE REACTIONS WAS DETERMINED FROM EQUATION 8

Temperature (K)	Reaction Time (days)	Reaction Time (sec)
1200	2.67×10^{-3}	230
3100	3.12×10^{-12}	2.7×10^{-7}
5000	2.24×10^{-14}	1.9×10^{-9}

900 °C were such that accurate rates could not be extracted. Second, and perhaps more serious in nature, is the fact that we have attempted to extrapolate kinetic data over a temperature range of about 2000 K, that is, from ~1000 K to ~3000 K. Such extrapolation is questionable even over a range of a few hundred degrees, and we are not aware of any chemical rate laws which take the same form over a range of more than a hundred or so degrees. When temperatures of ~3000 K are approached, we are dealing with the chemistry of excited states, which almost always display radically different kinetics from ground states of the same species. We must therefore conclude that the kinetic predictions made here are the best possible given the present data; however, application of these predictions to temperatures higher than ~1500 K is very questionable.

The need for kinetic data at temperatures approximating the bubble conditions is clear from the foregoing discussion. Experimental kinetics at these high temperatures with this system will probably have to be studied by atom beam techniques. A variable-temperature sodium beam incident on the mixed-oxide pellet under high-vacuum conditions with subsequent surface analysis of the pellet after different beam exposure times would yield empirical rate laws. Mass spectrometric detection of reflected reactants, products, and intermediates would provide additional information which would possibly lead to the elucidation of the reaction mechanism.

3.3.3 Environmental Implications

In the event that an HCDA occurs, and radioactivity from the vapor bubble is released to the atmosphere, the radioactivity will be dispersed downwind by the normal atmospheric mixing processes and will lead to the irradiation of man by the following pathways: 1) external radiation from the cloud as it passes overhead; 2) internal radiation from activity inhaled during the passage of the cloud; 3) external radiation from activity deposited from the cloud; 4) internal radiation from ingestion of contaminated water and foodstuffs; and 5) internal radiation from inhalation of resuspended activity. Irradiation from inhalation of resuspended activity, external radiation from the cloud, and external radiation from activity deposited from the cloud are not considered in this assessment; measures could be taken to limit irradiation by these routes. Moreover, the dose from inhalation of resuspended activity, even in the absences of countermeasures, is probably less than the uncertainty associated with the estimate of the dose from inhalation of activity in the cloud [36].

The results of this study show that aerosols in the respirable range 0.01 to 0.50 μm are produced, and that mixed sodium fuel or sodium actinide aerosols are formed. The solubility of PuO_2 has been shown to be enhanced in the lung when sodium is present with the PuO_2. Experimental evidence in animals has shown that inhaled polydisperse aerosols of mixed sodium and plutonium oxides are transported from the lungs to liver and bone to a greater extent than plutonium dioxide aerosols with similar aerodynamic-size distributions [37]. This increased transportability depends upon the ratio of sodium to plutonium in the aerosol. Experimental evidence in rats has shown that after six months, greater amounts of inhaled aerosols of sodium and mixed-oxide fast-breeder-reactor fuel (80% $^{238}UO_2$ -20% $^{239}PuO_2$) are transported from the lungs to the body, by a factor of up to 30, from the mixed sodium-fuel aerosol [Na: fuel mass ratio of above 12:1] than from an aerosol of fuel alone [38]. Various studies showed that when the atomic ratio of sodium to plutonium dioxide was greater than 10:1, the amount of plutonium translocated from the lung to extrapulmonary tissues was between 3% and 3.4% of the initial lung deposit up to one year after inhalation [36]. This is significant compared to the less than 0.5% of the initial plutonium lung deposit translocated one year after inhalation of plutonium dioxide aerosols alone [36].

HCDA aerosols inhaled by humans or animals could be expected to react the same way as sodium and mixed-oxide fuel. There would be a greater translocation of the plutonium from the lungs to other organs of the body.

The results of this study show that respirable mixed ($^{238}UO_2$-$^{239}PuO_2$) aerosols (0.01 to 0.50 μm) with and without sodium are soluble in simulated lung fluid (SLF). Without sodium 2.6% $\pm$ 1.5% of ^{239}Pu was soluble in SLF, and with sodium 5.5% $\pm$ 1.1% ^{239}Pu was soluble in SLF. This increased solubility with sodium is a factor of 2.1 times greater than without sodium.

Thus, during an HCDA the greatest potential hazard to man is the inhalation of these respirable $^{239}PuO_2$ aerosols. The majority of the uptake, 94.5%, would remain in the lung, and some would be transferred to the gastrointestinal tract by ciliary action of the lungs. The remainder of the uptake, 5.5% $\pm$ 1.1%, would be soluble and be translocated from the lung to the bone and liver. The actual risk factors for cancer could be influenced by medical treatments such as irrigation of the lungs to remove the insoluble ^{239}Pu and injections of complexing agents such as EDTA to eliminate the soluble ^{239}Pu. In either case, the inhalation of aerosols from an HCDA would definitely increase the risk factor of cancer in the lung, bone, and liver. The actual risk factors could be calculated from the total exposure and from the amount retained in the body after medical treatment.

The ingestion of ^{239}Pu from foodstuffs and water is another potential hazard to man from an HCDA. Foodstuffs have been shown to absorb 1×10^{-2} less than the original amount of ^{239}Pu deposited on the surface [39]. This amount then decreases to a factor of 1×10^{-6} after a rain [39]. Thus, the risk of ingestion to man through foodstuffs is not very great, especially after a rain.

The results of this study show that ^{239}Pu is soluble in water with and without sodium present. Without sodium present, 5.3% $\pm$ 1.5% of the ^{239}Pu aerosols are soluble in water, and with sodium, 8.7% $\pm$ 2.4% of ^{239}Pu aerosols are soluble in water. Thus, during an HCDA, 91.3% of the ^{239}Pu would be insoluble, and 8.7% $\pm$ 2.4% would solubilize in the water supply. The insoluble ^{239}Pu has been shown to fall through the water and become entrapped and mixed with the sediment on the bottom [39]. The soluble ^{239}Pu has been shown to behave in the same way as the insoluble ^{239}Pu after a few days and become mixed with the sediment [39]. The soluble ^{239}Pu left in the water is a factor of 1×10^{-8} less than the original amount of ^{239}Pu solubilized [39]. Thus, the risk of ingestion of ^{239}Pu from foodstuffs and water are very low in the event of an HCDA. The greatest risk from an HCDA is from the inhalation of respirable ^{239}Pu aerosols mixed with sodium.

The actual risk factors for cancer would depend on several factors, such as total exposure and reaction of the individual to medical treatment to eliminate both the soluble and insoluble ^{239}Pu from the body.

3.3.4 Recommendations for Future Work

The key to understanding the chemistry of HCDA and core-melt aerosols is the proposed physical and chemical models for comparing calculated to experimental results. In order to calculate the quantities associated with any model one must have the appropriate thermodynamic and kinetic data available. The unavailability of these data has been a limiting constraint in HCDA and core-melt aerosol chemistry. We have been able, to a limited extent, to assess the applicability of an equilibrium thermodynamic model to sodium uranate formation. The disagreement with experiment shows that sodium uranate formation is not a thermodynamically controlled process. The thermodynamic results were of use, however, in rationalizing the experimental results in terms of a cooling curve/seed-out mechanism. Chemical kinetics data on sodium uranates and plutonates at realistic HCDA temperatures would be very helpful in understanding HCDA aerosol chemistry. In order to give a concise guide to what thermochemical and kinetic data have been determined and to what areas emphasis should be directed, the following outline was constructed.

SUMMARY OF THERMOCHEMICAL AND KINETIC DATA ON THE Na-U-O AND Na-Pu-O SYSTEMS

Core-Melt Temperature Range (~700 to 900 °C)

I. Thermochemical Data
   A. Systems studied - Na-U-O
      1. Type of data - heats of formation for sodium uranates
      2. Method - high-temperature Knudsen effusion/mass spectrometry
      3. Reference - J. E. Battles, W. A. Shinn, and P. E. Blackburn, *J. Chem. Thermo.*, *4*, 425 (1972).

   B. Systems in need of study: Na-PuO
      1. Type of data needed - heats of formation and heat capacities
      2. Probable best method - high temperature mass spectrometry
      3. Feasibility - feasible by same method as above (I-A-3).

II. Chemical Kinetic Data
   A. Systems studied - mixed oxide (Pu/U+Pu=0.20) and sodium
      1. Type of data - rates determined from volume change as a function of time data
      2. Method - metallographic microscopy
      3. Reference - Q. E. Martin and J. Schilb, in *ANL Fuels and Materials Chemistry Semiannual Report*, Argonne National Laboratory, Chemical Eng. Div. (July-December 1972), pp. 4-9.

   B. Systems in need of study - PuO_2/Na, UO_2/Na, more accurate data needed on mixed oxide/Na system
      1. Type of data - rate constants for uranate and plutonate formation as functions of temperature
      2. Probable best method - metallographic microscopy
      3. Feasibility - very feasible; same methods as used by Martin and Schilb will work with single oxides; accuracy of method can be improved by more careful experimental design.

HCDA Temperature Range (~900 to 2800°C)

I. Thermochemical Data
   A. Systems studied - Na-U-O (extrapolation of data to highest part of temperature range may be questionable)
      1. Type of data - heats of formation
      2. Method - mass spectrometry
      3. References - J. E. Battles, W. A. Shinn and P. E. Blackburn, *J. Chem. Thermodynamics, 4,* 425 (1972).

   B. Systems in need of study - Na-Pu-O at high end of temperature range
      1. Type of data - heats of formation, high temperature heat capacities
      2. Method - mass spectrometry/calorimetry
      3. Feasibility - experimentally feasible.

II. Chemical Kinetic Data
   A. Systems studied - none
   B. Systems in need of study - Na-U-O, Na-Pu-O
      1. Type of data - rate constants and/or cross sections for uranate formation reactions and formation of intermediate gaseous species.
      2. Method - high temperature mass spectrometry, atom beam experiments, surface analysis.
      3. Feasibility - feasible, but requires large initial outlay for instrumentation and an in-depth research effort to achieve enough results to make reliable predictions.

In light of recent de-emphasis of the HCDA scenario and the high cost in both time and money to obtain kinetic data in the HCDA temperature range, these experiments are not recommended. Future efforts would be best directed toward collecting thermochemical data on the Na-Pu-O system by mass spectrometric methods, similar to those used by Battles, et al., on Na-U-O, and toward collecting rate data on U, Pu, mixed-oxide systems by microscopic volume change measurements, essentially an extension of the work of Martin and Schilb. Both these efforts would generate data applicable to the core-melt temperature range. Since the methods are well established (not state-of-the-art), and the volume of data required is not too large, these endeavors would be markedly more cost effective than the atom beam experiments of HCDA-II-B would be.

4. Aqueous PuO_2 Solubility Studies

4.1 Introduction

During an HCDA, considerable quantities of vaporized UO_2, PuO_2, and sodium could escape from the reactor containment to the environment. The inhalation of aerosols of $^{239}PuO_2$ and the eventual contamination of ground water are of great concern from the aspect of biological safety because of the toxicological effects of $^{239}PuO_2$ in water and simulated lung fluid. Therefore the enhanced solubility of plutonium with sodium present is valuable information that can be used to assess the biological risk factors for an HCDA.

Raabe and Fleischer have shown that respirable $^{239}PuO_2$ particles <0.3 μm in diameter appear to dissolve in water [40]. They theorize that the $^{239}PuO_2$ particles "dissolve" in water by a process of alpha-decay-induced fragmentation, probably caused by the heavy, recoiling nuclei.

Allen et al. studied the dissolution characteristics of Liquid Metal Fast Breeder Reactor (LMFBR) sodium-fuel aerosols [42]. In the distilled-water dissolution studies of sodium-fuel aerosols, the amount of soluble plutonium was dependent on the sodium-fuel ratio. Increasing the amount of sodium leads to an increase in the amount of soluble plutonium. Dissolution studies of sodium-fuel aerosols using simulated lung fluid also show that the amount of soluble plutonium is dependent on the sodium-fuel ratio. Plutonium was markedly less soluble in simulated lung fluid than in distilled water.

This portion of the report shows the results of solubility studies of $^{239}PuO_2$ aerosols in water and in simulated lung fluid. The data were collected from systems comprising mixed oxide fuel and reactor structure materials. The aerosols were collected with and without sodium in both cases.

4.2 Experimental

The radioactive pellets used for this study were composed of depleted uranium dioxide, plutonium dioxide, and reactor structural materials mixed to the following compositions (in weight percent): a) 75% UO_2/PuO_2 -25% 316 stainless steel, and b) 75% UO_2/PuO_2 -25% 316 stainless steel -Na(liquid). The materials used were mixed and pressed into pellets under the same conditions as described previously in this report. Sodium was introduced into a depression prepared in the center of the pellets. The pellets were heated to melt the sodium in the depression just before laser heating.

In this study the pellets were heated with the rail laser fitted with a neodymium glass rod as shown in Figure 4. The stub support was removed from the laser heating fixture, and the vaporized portion of the pellet was condensed on glass slides that were suspended under the quartz top. Figure 26 illustrates the modified static laser heating fixture.

The condensate was removed from the glass slides and placed in centrifuge tubes. Distilled water and simulated lung fluid (which was prepared by a recipe described by Kanapilly, et al.) were added (~10 ml), and the tubes were centrifuged for 20 min [43]. The distilled water and the simulated lung fluid were decanted and analyzed for plutonium-239 by alpha scintillation counting techniques. The residual particles, from the test tube, were transferred into beakers containing 5N HCl and three drops of HF. The acid solution was evaporated to near dryness three times to ensure the dissolution of the residue. The solutions were diluted with distilled water (~10 ml) and analyzed for plutonium-239 by alpha scintillation counting.

4.3 Results

Aerosols formed in this study were primarily assessed by examining the dissolved products by alpha scintillation counting techniques. The pellet compositions, total mass of plutonium-239 vaporized, total mass of plutonium-239 dissolved in distilled water and simulated lung fluid, and the percent of plutonium-239 dissolved in distilled water and simulated lung fluid are summarized in Tables 8 and 9. The results show that sodium enhances the solubility of plutonium-239 in both distilled water and simulated lung fluid by about a factor of 2. In both cases the solubility of plutonium-239 was greater in distilled water than in simulated lung fluid.

4.4 Discussion

Should an HCDA occur and if the vapor bubble containing fuel, sodium, and reactor structural materials escapes the containment, the inhalation of plutonium-239 and the adsorption of plutonium-239 into the water supply would be of vital concern. Originally, the HCDA aerosols were believed

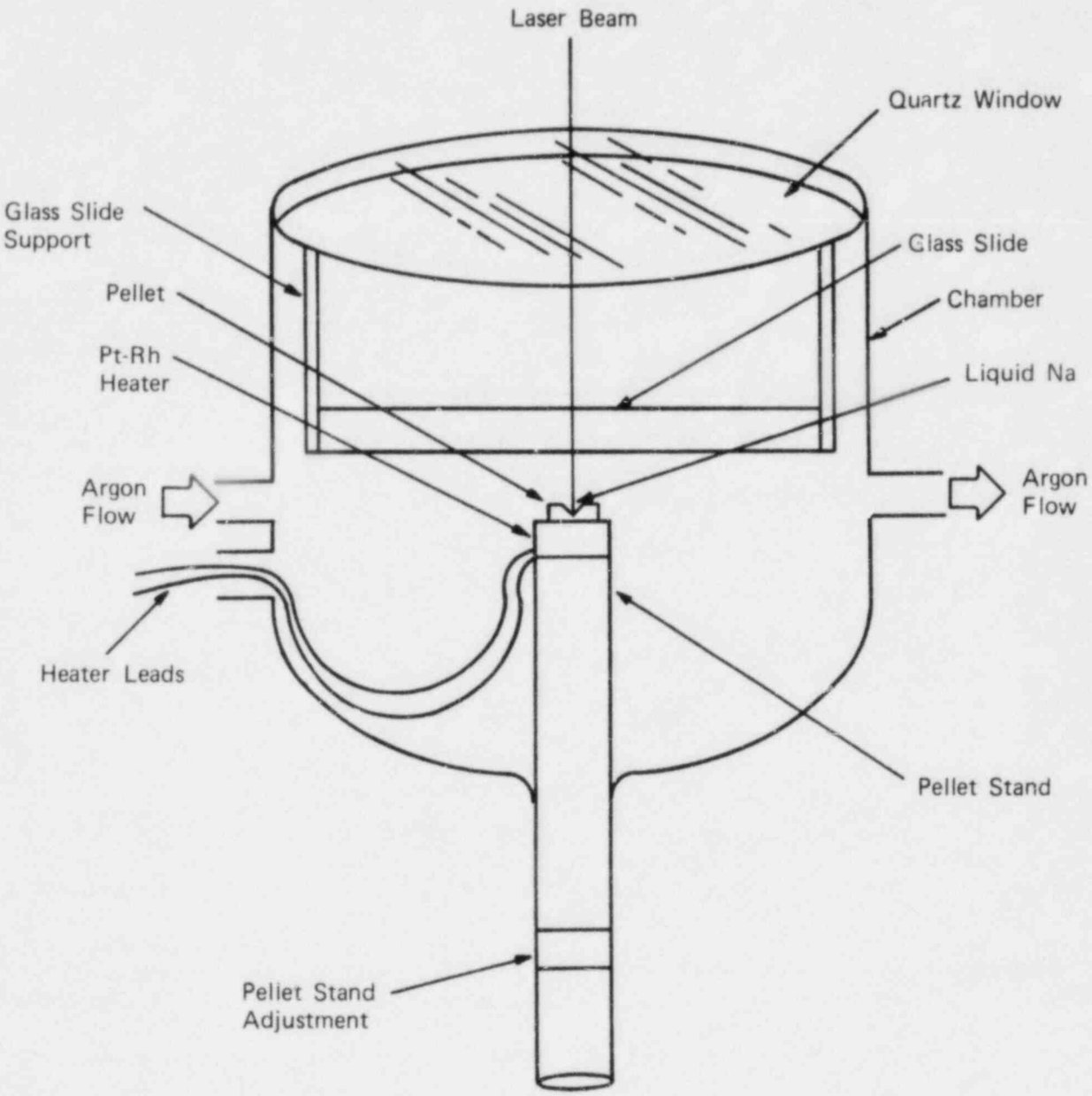

FIGURE 26 - Modified static laser heating system fixture which permits inert-gas laser heating.

Table 8 - PuO_2 SOLUBILITY IN WATER

System	Trial A	Total Mass ^{239}Pu (μg)	Soluble Mass ^{239}Pu (μg)	^{239}Pu Soluble (%)
75% UO_2/PuO_2-25% SS	1	45.0	1.6	3.6
75% UO_2/PuO_2-25% SS	2	51.7	3.1	6.0
75% UO_2/PuO_2-25% SS	3	57.8	3.6	6.2
	Mean	51.5	2.8	5.3
	Std.Dev.	6.4	1.0	1.5
75% UO_2/PuO_2-25% SS-Na	1	23.5	2.2	9.5
75% UO_2/PuO_2-25% SS-Na	2	24.5	1.7	.8
75% UO_2/PuO_2-25% SS-Na	3	66.3	4.8	7.2
75% UO_2/PuO_2-25% SS-Na	4	50.4	3.2	6.4
75% UO_2/PuO_2-25% SS-Na	5	24.1	3.1	12.9
75% UO_2/PuO_2-25% SS-Na	6	12.1	1.1	9.1
	Mean	33.5	2.7	8.7
	Std.Dev.	20.4	1.3	2.4

to consist of insoluble $^{239}PuO_2$. The results from this study show that $^{239}PuO_2$ aerosols are soluble in distilled water and simulated lung fluid.

The $^{239}PuO_2$ average solubility in distilled water without sodium was 5.3% ± 1.5% and with sodium was 8.7% ± 2.4%. The $^{239}PuO_2$ average solubility in simulated lung fluid without sodium was 2.6% ± 1.5% and with sodium was 5.5% ± 1.1%. The results from the simulated lung fluid study compare very favorably with the average fractional dissolution of 2.44% per day and the maximum of 5.2% obtained by Raabe et al. from their *in vitro* solubility studies [44]. The main differences in the studies were: 1) the method of aerosol collection; 2) this study used mixed oxide fuel, reactor structural material, and sodium, not just $^{239}PuO_2$; and 3) the dissolution was done at 25° C, compared to 37° C. The *in vitro* dissolution data were used to estimate the initial ^{239}Pu lung burden, Q_o, using Healy's method [44]. For 2.44% solubility the lung burden, Q_o, was 411 nCi, and for 5.0% solubility the lung burden was 472 nCi. These values were, in general, in agreement with the estimate of Q_o, 450 nCi, obtained by whole body counting [44]. If Healy's method for estimation of the initial ^{239}Pu lung burdens is used and the same assumptions are applied as the *in vitro* study, the dissolution values of 2.6% ± 1.5% and 5.5% ± 1.1% from this study would be slightly less (386 nCi and 419 nCi) but would compare favorably with the *in vitro* lung burden estimations of 411 nCi and 472 nCi.

Table 9 - PuO_2 SOLUBILITY IN SIMULATED LUNG FLUID

System	Trial	Total Mass ^{239}Pu (μg)	Soluble Mass ^{239}Pu (μg)	^{239}Pu Soluble (%)
75% UO_2/PuO_2-25% SS	1	38.4	1.2	3.1
75% UO_2/PuO_2-25% SS	2	33.2	1.1	3.3
75% UO_2/PuO_2-25% SS	3	42.5	2.4	5.6
75% UO_2/PuO_2-25% SS	4	46.4	0.6	1.3
75% UO_2/PuO_2-25% SS	5	32.0	0.5	1.6
75% UO_2/PuO_2-25% SS	6	24.0	0.4	1.7
75% UO_2/PuO_2-25% SS	7	101.1	1.2	1.2
75% UO_2/PuO_2-25% SS	8	102.9	1.6	1.6
75% UO_2/PuO_2-25% SS	9	40.3	1.7	4.2
	Mean	51.2	1.2	2.6
	Std.Dev.	29.5	0.6	1.5
75% UO_2/PuO_2-25% SS-Na	1	55.1	3.2	5.8
75% UO_2/PuO_2-25% SS-Na	2	18.0	0.7	3.9
75% UO_2/PuO_2-25% SS-Na	3	21.7	1.3	6.0
75% UO_2/PuO_2-26% SS-Na	4	17.6	1.1	6.3
	Mean	28.1	1.6	5.5
	Std.Dev.	18.1	1.1	1.1

The solubility of $^{239}PuO_2$ in distilled water with sodium present compares favorably with the dissolution characteristic of the LMFBR fuel-sodium aerosols found by Allen et al. [42]. The study showed that the solubility of $^{239}PuO_2$ in distilled water was dependent upon the sodium-fuel ratio, and that nearly all of it dissolves in the first 30 min; after that, the plutonium-239 is relatively insoluble in distilled water. In this study the 8.7% ± 2.4% solubility with sodium present compares closely with the 4:1 sodium-to-fuel ratio value of 10.0% of Allen et al. The $^{239}PuO_2$ solubility in distilled water with no sodium present compared favorably with the results of Fleischer and Raabe [40]. The value of 5.3% ± 1.5% for this study was ~1.8 times greater than the 3.0% for the 0-1 hr value and was about the same as the 5.6% for the 1-24 hr value reported by Fleischer and Raabe [40]. These values were obtained by exposing $^{239}PuO_2$ particles of geometric diameter 0.3 μm to 100 ml of high purity water for 1 and 23 hr durations. A third value of 8.3% was obtained upon exposure to

high purity water for a 24-hr time span. This value of 8.3% is a factor of ~1.7 times greater than the value of 5.3% ± 1.5% for this study. The exact mechanism of dissolution reported by Fleischer and Raabe has not been resolved but their values indicate that the solubility of $^{239}PuO_2$ in high purity water is time dependent.

4.5 Conclusions

This study shows that $^{239}PuO_2$ aerosols (0.01 to 0.5 μm) from mixed oxide fuel are soluble in simulated lung fluid. With sodium present, the solubility is 5.5% ± 1.1%, and with no sodium present, 2.6% ± 1.5%. In an HCDA the greatest risk and the potentially most dangerous time is the inhalation exposure period for these aerosols. Calculations from Healy's equation show that the expected lung burden upon exposure to these aerosols would range from 385 to 419 nCi. From these initial results and the estimation of exposure time, the expected translocation of plutonium-239 from lung to blood and then to bone and liver could be calculated. These values could be used to assess the risk factors of exposure time and inhalation of plutonium-239 for a real case scaled up LMFBR safety analysis.

This study also shows that $^{239}PuO_2$ aerosols (0.01 to 0.5 μm) from mixed oxide fuel are soluble in distilled water. With sodium present, the solubility is 8.7% ± 2.4%, and with no sodium, 5.3% ± 1.5%. The next most important risk to man from an HCDA release of these particles, after inhalation, would be the fallout and subsequent adsorption into the water and food pathways. The worst case pathway would be via the aerosols being deposited directly in streams and rivers that are used for drinking water and for fishing (assuming that the fish are eaten). The second case would be the deposition of the aerosols on vegetation and sediment. The aerosols could then be dissolved in ground water and enter the water pathway or be ingested or inhaled from the vegetation or sediment.

A study of $^{238}PuO_2$ in the environment showed that soluble plutonium-238 entering these pathways was 10^4 to 10^5 times less than the original deposited concentration [39]. As $^{239}PuO_2$ is ~300 times less active than $^{238}PuO_2$, the risk for human ingestion by these pathways should be 10^4 to 10^5 less if not more than the original concentrations of 8.7% ± 2.4% and 5.5% ± 1.1% are present.

In conclusion, the greatest risk from aerosols released from an HCDA are the inhalation of respirable particles and their solubility in lung fluid and transfer by the blood to liver and bone. The lung burden (Q_0) can be calculated from the data presented as well as estimations of transfer to the bone and liver. Assessment of the risk factors can be made based on the concentration and exposure time to these respirable aerosols.

The risk factors for ingestion of respirable aerosols from an HCDA, after fallout on vegetation, soil, and waterways, are 10^4 to 10^5 less than the original concentration deposited. Though the risk factors for ingestion after fallout are low, it follows that the potential and long-term fate of these respirable aerosols in the environment would merit careful attention and monitoring, since the environmental distribution and dispersibility of the aerosols must depend sensitively on their size distribution. The uptake in the plant and water chain could be markedly affected by the presence of respirable aerosols.

5. PuO_2/Na Solubility Studies

5.1 Introduction

In the case of a severe HCDA, with core rupture of a sodium-cooled LMFBR, the core could melt through the reactor tank and be contained in an ex-vessel core catcher or melt through the core catcher to the cement building floor. In either case, it would be covered with hot, possibly boiling, sodium.

During the process of core meltdown, considerable quantities of fuel particles and fission products would be suspended or dissolved in liquid sodium. Some of the fission

products and also fuel aerosols or reaction products of fuel-sodium reaction are subsequently vaporized into the free volume of the reactor and then released into the reactor containment. For the estimation of activity concentration in the containment, it is important to know the quantities of sodium, fuel, and fission products that are released from hot or boiling sodium pools. This information becomes especially important if reactor containment is breached.

Even at the core rupture point (temperatures as high as 6000 °C), it is assumed that most of the evaporated or molten fuel is still in the oxidized state [8]. Some of the evaporated fuel recondenses to particles and is suspended in the sodium. Conservative calculations here have shown that up to 7-8 kg of fuel might be suspended in 1 m^3 of sodium

The release of fuel from sodium into the gas phase is possible in two ways: particles or aerosols are ejected mechanically from sodium, for example, by collapsing bubbles, or, after sodium-fuel reaction, as a compound with a higher evaporation rate than the UO_2 and PuO_2 fuel.

The reaction product, sodium uranate (Na_3UO_4), is well characterized and is stable in the system Na-UO_2 -Na_3 UO_4 at oxygen concentrations of 0.4 to 0.9 ppm in sodium and at temperatures above 500 °C [45].

The counterpart sodium plutonate, Na_3PuO_4, and its mixed actinide analog, $Na_3(U,Pu)O_4$, are not as well characterized as Na_3UO_4.There have been only a few calculations on fuel release from burning sodium pools. It is estimated that 1 x 10^{-5}% of PuO_2 contained in the pool may be released to the environment [46].

Sodium vapor was released from a boiling sodium pool into a nitrogen atmosphere at a rate of 85 kg of Na/m^2·h. Decontamination factors for uranium release from sodium pools were measured at between 1 x 10^3 and 5 x 10^3 for sodium containing 1.0 wt % of UO_2 powder. No significant temperature dependence of the decontamination factor between 500 and 900 °C was found. Sodium and uranium were found to evaporate separately into the atmosphere [46].

To allow determination of the amount of $^{239}PuO_2$ that would be released from a hot sodium pool, a study was performed to determine the solubility of $^{239}PuO_2$ in sodium. The solubility would give an estimate of the amount of sodium-fuel reaction product available for evaporation from the sodium pool. From these results the concentration of $^{239}PuO_2$ that did not dissolve could be calculated. The undissolved $^{239}PuO_2$ would be available for release from the sodium pool by mechanical methods. The effect of temperature and oxygen content on the solubility of $^{239}PuO_2$ in sodium was also measured.

5.2 Experimental

The plutonium dioxide and sodium metal used for this study were the same as those materials referred to in previous sections of this report. The argon atmosphere glovebox used for this study contained < 10.0 ppm oxygen and 1.0 ppm in moisture content. In this study a 10:1 ratio of sodium to $^{239}PuO_2$ fuel was loaded into stainless steel and nickel capsules that were 6.35 cm long by 0.64 cm in diameter. Figure 27 illustrates the capsule design. In the oxygen dependence studies, high purity anhydrous sodium oxide (Na_2O) was weighed to obtain 1000, 1400, and 10,000 ppm of oxygen based on the total weight of sodium and fuel in the capsule. The $^{239}PuO_2$ fuel was weighed and transferred through a small glass funnel to the bottom of the capsule. In the oxygen dependence studies, first Na_2O was weighed and transferred through a funnel to the bottom of the capsule. Then sodium was weighed, trimmed of any oxide, rolled, dropped into the capsule, and tamped against the fuel at the bottom of the capsule. A nickel slug or a stainless steel sphere was dropped into the capsule, which was then sealed by torquing down a stainless steel socket head screw. When the screw bottomed out, it was 1.27 cm below the top of the capsule. The top of the capsule was then crimped and welded to completely seal the capsule. The capsules were placed in a furnace in the inert glovebox. No more than eight capsules were

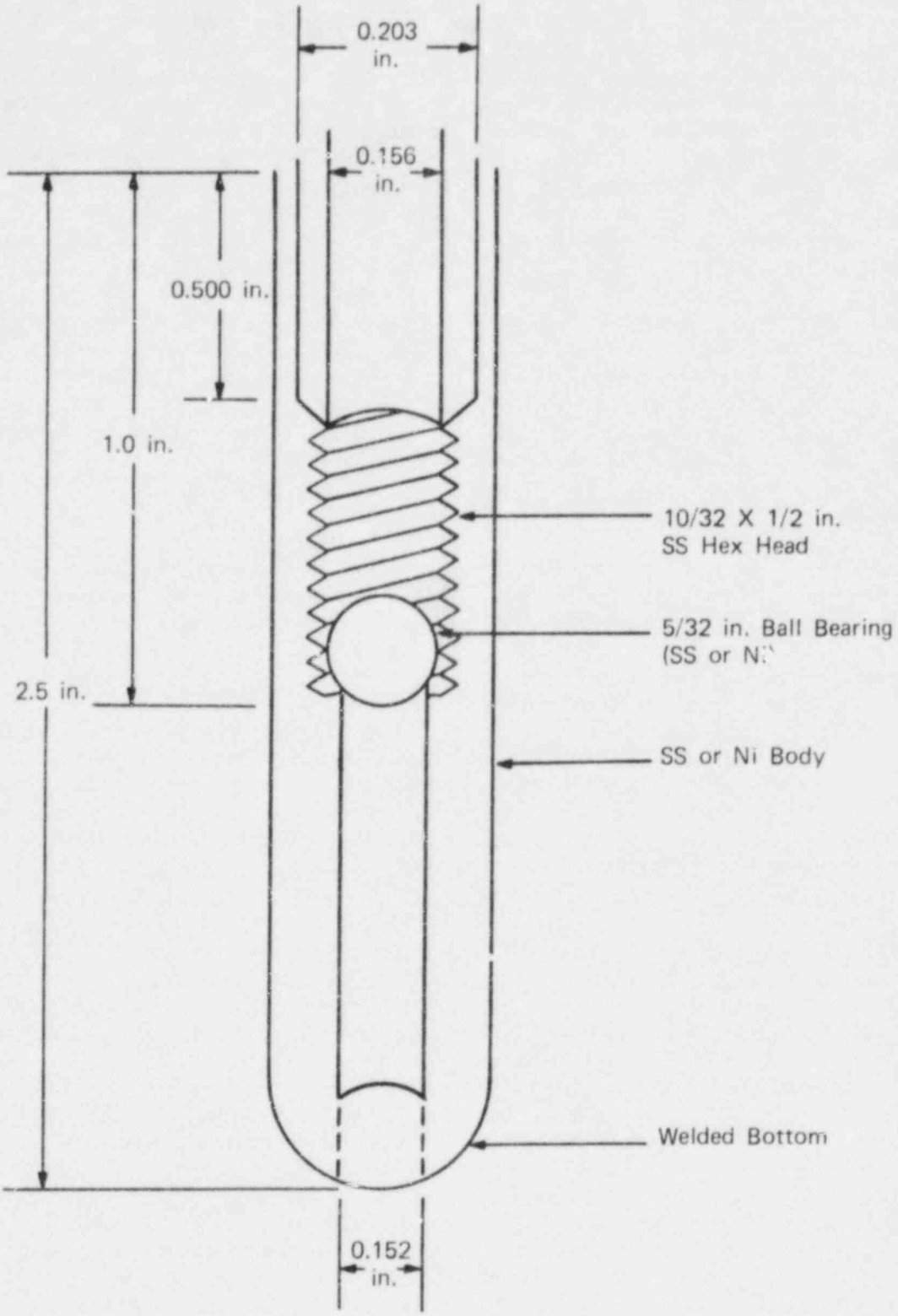

FIGURE 27 - Capsule design used for the studies of the solubility of $^{239}PuO_2$ in sodium.

loaded into the furnace at any one time for heat treatment. Figure 28 is a schematic of the furnace and glovebox used for the study.

The capsules were thermally soaked for three days at temperatures of 500, 600, 700 and 800 °C. After the thermal soak was completed, the capsules were quenched in oil and then cut open with a pipecutter. The cuts were made 2.5 cm below the top and 0.6 cm above the bottom of the capsule. The sodium was pushed out of the capsule with a stainless steel rod. The sodium-fuel sample was weighed, placed in a polyethylene screw cap bottle, and dissolved in 10 ml of absolute alcohol. The samples were then filtered through *#41* Whatman filter paper into 25-ml volumetric flasks. The solutions were transferred to polyethylene screw-capped bottles and counted for total plutonium-239 by alpha liquid scintillation counting techniques.

In the oxygen dependent studies, nickel capsules and slugs were used because the literature suggested that stainless steel containment capsules act as an oxygen getter for liquid alkali metals [47]. Thus, the studies that were conducted in stainless steel capsules with the addition of oxygen, as Na_2O, actually represent zero oxygen level. Therefore, all results acquired from the stainless steel capsules can be considered at the zero oxygen level.

5.3 Results

Results for the two phases of the study were primarily assessed by alpha scintillation counting techniques. The capsule material, weights of $^{239}PuO_2$, sodium, sodium oxide, temperatures, thermal soak time, oxygen added, $^{239}PuO_2$ soluble in sodium, and the standard deviation (σ) are summarized in Tables 10 and 11. The results (shown in Figures 29 and 30) do not reveal any significant (greater than noise level) dependence of temperature or oxygen content on the solubility of $^{239}PuO_2$ in sodium.

The reason for scatter of the data is not known but is suspected to be caused by colloidal suspension of $^{239}PuO_2$. To investigate the validity of this hypothesis, in future experiments the alcohol extraction solutions could be filtered through milliapore filters or reacted with some compound, such as $Al_2(SO_4)_3$, to precipitate the colloidal particles. In either case, scintillation counting results of the solution after treatment would change significantly if the hypothesis is true.

All experimental data were subjected to a statistical Q-test, which rejects outlying values at a 90% confidence level, before the average values and standard deviations were computed.

5.4 Discussion

Should a severe HCDA occur, the core could melt and be contained in an ex-vessel core catcher or melt through the core catcher to the cement building floor. In either case, this fuel would be covered by at first hot and then boiling sodium. Before an accident, the reactor would contain 20 tons of fuel and 5,500 tons of sodium [36]. The 40,000 lb of fuel at the 80/20% ratio of UO_2/PuO_2 would contain 8000 lb of $^{239}PuO_2$ and 11 million lb of sodium. If a 10% burnup of the fuel was considered during the HCDA, then 7,200 lb of $^{239}PuO_2$ would be available in the core to dissolve in the sodium. This dissolved $^{239}PuO_2$ could then be vaporized with the sodium and escape into the reactor containment or possibly to the environment.

If the highest solubility of $^{239}PuO_2$ in sodium is 48.0 $\pm$ 41.0 ppm, then the highest (worst case) solubility of $^{239}PuO_2$ in sodium would be 89.0 ppm (9×10^{-3} or 0.009%). For ease in mathematical computation, the solubility of $^{239}PuO_2$ in sodium is 0.01%. Thus, of the 7,200 lb of $^{239}PuO_2$ available, 0.72 lb. (0.33 kg) of $^{239}PuO_2$ would dissolve in the sodium and vaporize with it. This would be the maximum amount of ^{239}Pu that could escape to the environment. Because of the low boiling point of sodium (900 °C), however, the chances are very good that the sodium will condense onto colder surfaces and be contained in the reactor containment building. Thus, the most exposure to man of the 0.33 kg of ^{239}Pu would be to the personnel involved in the cleanup and decontamination

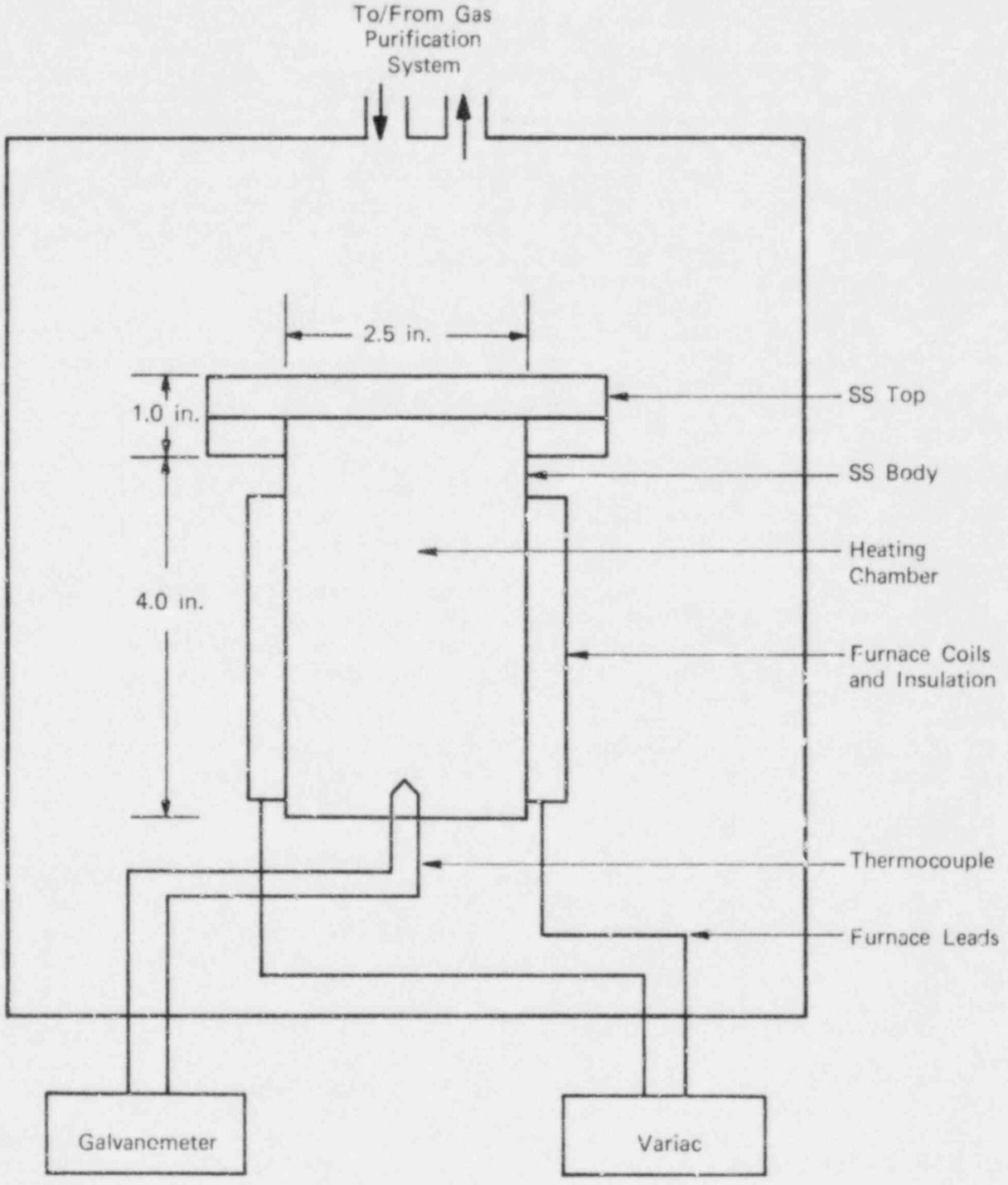

FIGURE 28 - Furnace and glovebox used for the studies of the solubility of $^{239}PuO_2$ in sodium.

Table 10 - SOLUBILITY OF $^{239}PuO_2$ in SODIUM AT VARIOUS TEMPERATURES

Type of Capsule	Trials	Number of Samples	Wt. of $^{239}PuO_2$ (g)	Wt. of Na (g)	Temp. (°)	Thermal Soak Time (days)	Average Solubility $^{239}PuO_2$ (ppm)	Std.Dev. (ppm)
SS	1	5	0.03	0.30	500	3	38.6	14.4
SS	2	5	0.03	0.30	600	3	24.6	12.9
SS	3	5	0.03	0.30	700	3	48.0	40.9
SS	4	8	0.03	0.30	800	3	30.5	29.0

Table 11 - SOLUBILITY OF $^{239}PuO_2$ IN SODIUM AT SEVERAL OXYGEN LEVELS

Type of Capsule	Trials	Number of Samples	Wt. of $^{239}PuO_2$ (g)	Wt. Of Na (g)	Wt. of Na_2O (g)	Oxygen Level (ppm)	Temp. (°C)	Thermal Soak Time (days)	Average Soiubility $^{239}PuO_2$ (ppm)	Std.Dev. (ppm)
Ni	1	5	0.03	0.30	0.0012	1000	500	3	36.8	47.8
Ni	2	8	0.03	0.30	0.0016	1400	500	3	38.6	40.0
Ni	3	5	0.03	0.30	0.0012	1000	800	3	28.8	11.9
Ni	4	6	0.03	0.30	0.012	10000	800	3	20.9	10.3
SS	5	4	0.03	0.30	0.0012	1000	800	3	21.2	25.8
SS	6	4	0.03	0.30	0.012	10000	800	3	27.1	25.9

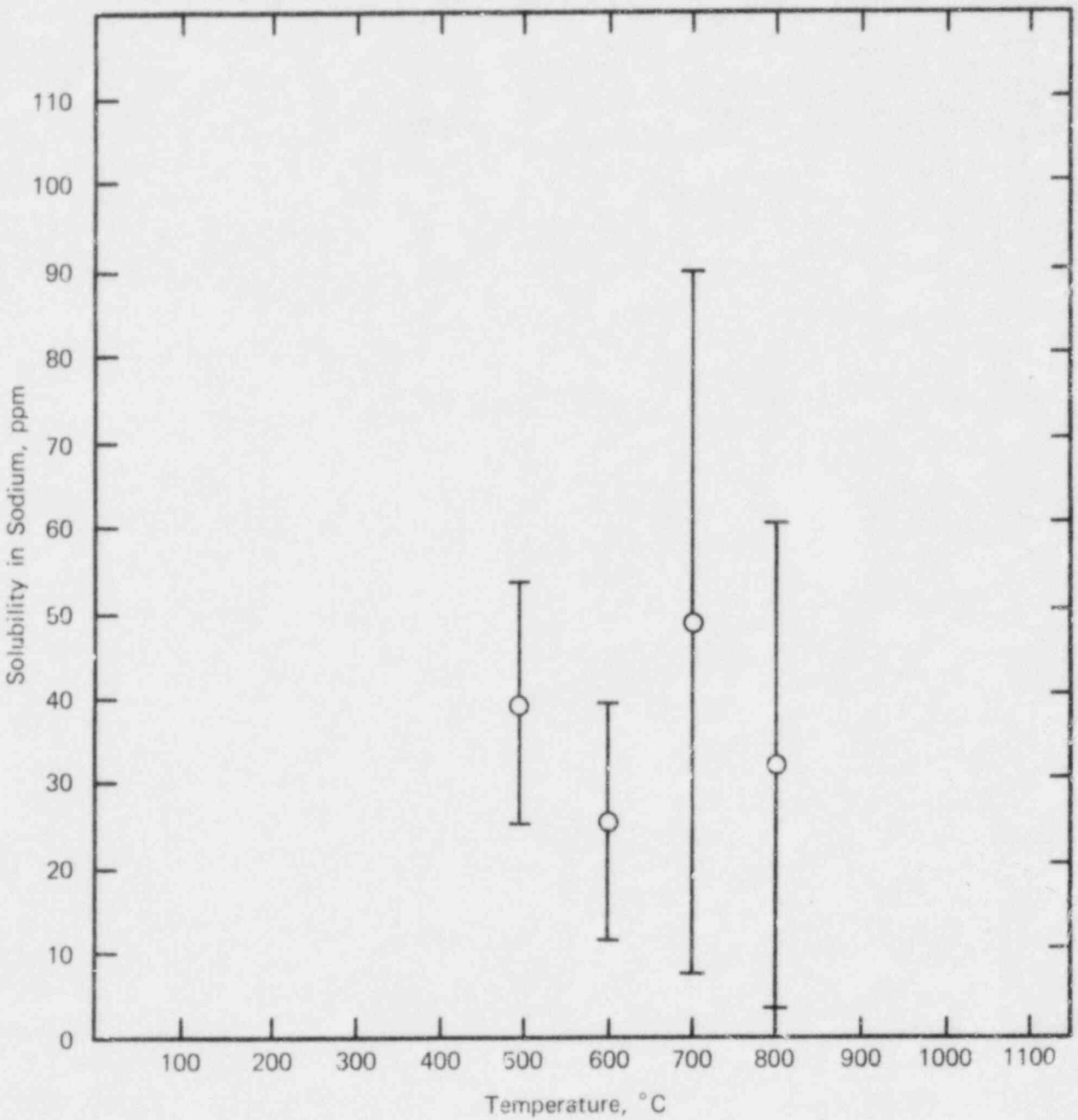

FIGURE 29 - Graphical representation of solubility as a function of temperature.

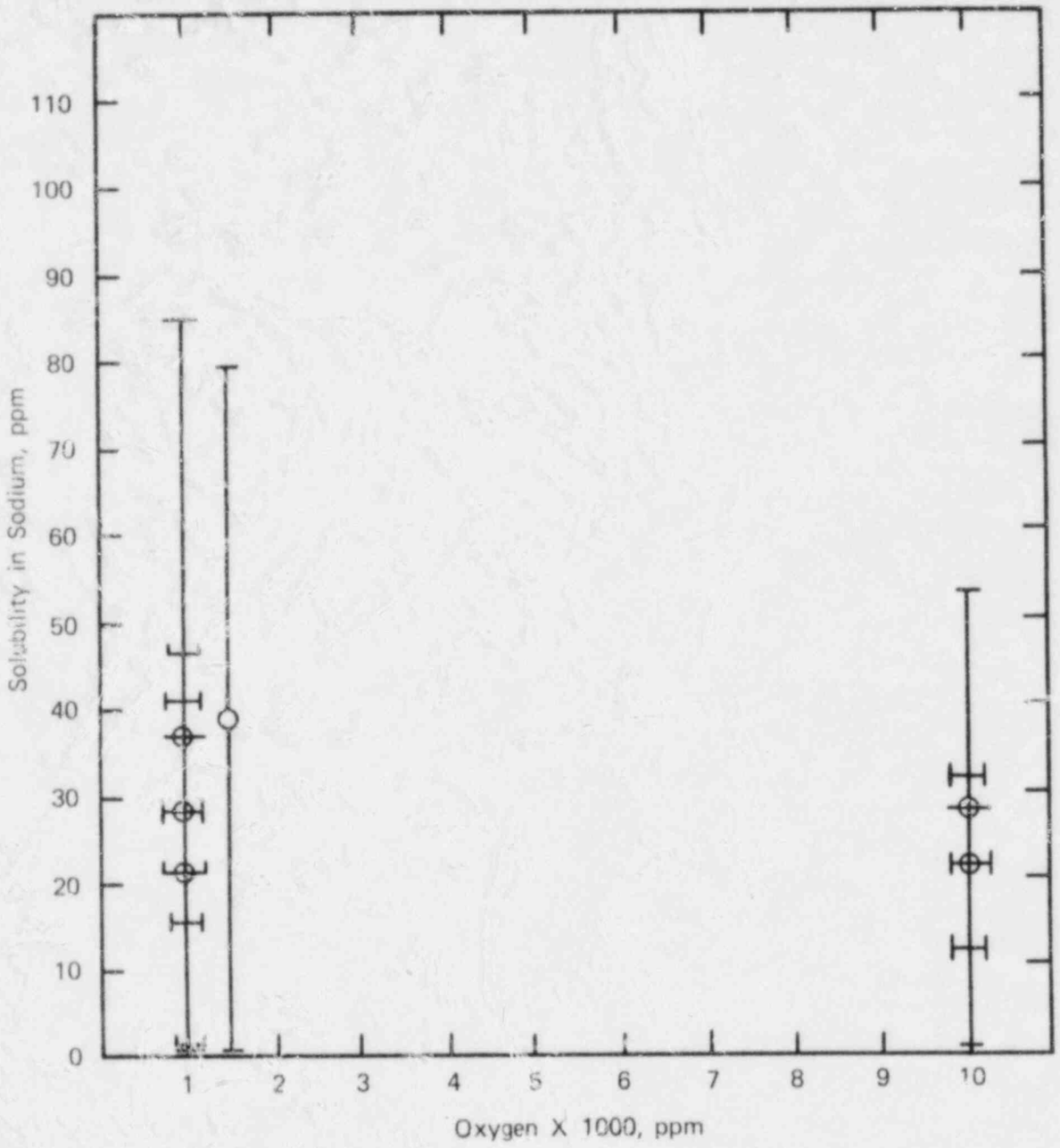

FIGURE 30 - Graphical representation of solubility as a function of oxygen content.

of the reactor facility. Although a single exposure of 0.33 kg under the right circumstances could have severe consequences to the human population and the environment, by comparison with an HCDA for a 10% burnup, which could possibly release 800 lb (364 kg) ^{239}Pu, the exposure potential from soluble ^{239}Pu in sodium would be a factor of approximately 1 x 10^3 less than the potential exposure from an HCDA. This factor could change if the escape of $^{239}PuO_2$ from the boiling sodium by mechanical means was greater by a factor of 10 than the 0.33 kg from dissolved ^{239}Pu. Studies that would simulate the energetics of the boiling sodium would have to be made to obtain the necessary data. These data could be scaled up to the reactor conditions or used with a computer code to estimate the amount of $^{239}PuO_2$ that would escape by mechanical means.

This study does not consider the possibility that the core could melt through the core catcher to the concrete floor. Studies have shown that hot sodium reacts rather violently with concrete [48]. This could cause the concrete to erode and allow the fuel and sodium to escape into the environment to the ground. This would be another serious problem that would have to be solved during cleanup and decontamination.

5.5 Conclusions

The greatest solubility of $^{239}PuO_2$ (worst case) in sodium is approximately 100 ppm or 0.01%. From the reactor conditions, 0.33 kg of $^{239}PuO_2$ would be available to escape from the sodium by vaporization. Since there is no solubility dependence on temperature or oxygen content, a breach in the reactor containment building would not change the solubility. Although a breach would increase the chances of the dissolved ^{239}Pu to escape to the environment, because of the low boiling point of sodium (900 °C) the sodium containing ^{239}Pu will condense on the cooler surface inside the containment building. From a safety standpoint the potential exposure from the dissolved ^{239}Pu escaping from the sodium will be a factor of 1 x 10^3 less formidable than the HCDA event. Should the HCDA event be contained in the reactor building, then the additional dissolved ^{239}Pu escaping from the boiling sodium will be insignificant.

6. Acknowledgements

The authors thank E. Stacy who operated the transmission and scanning electron microscopes and who photographed the aerosol particles and electron diffraction patterns which were used in this study, D. R. Kaser who helped design and set up the radioactive laser facility, W. D. Sibert and W. H. Jones who adapted the laser to the reconditioned laser rod, and D. B. Sullenger and D. R. Rohler who interpreted the x-ray diffraction data. We would also like to thank C. E. Burgan, S. B. Wells, and W. B. Cartmill for the design, fabrication, heat treating, and welding of the test capsules. We are grateful to R. E. Sprague and V. L. George for the use and maintenance of the inert atmosphere welding glovebox.

References

1. T. S. Kress, G. W. Parker, and M. H. Fontana, "Work Plan: Transient Release from LMFBR Fuel," ORNL-TM-4875 NRC-7, Oak Ridge National Laboratory (September, 1975).

2. J. Graham, "Liquid Metal Fast Breeder Reactor Safety," presented at the National Meeting of the AIChE on Fast Breeder Development, Pittsburgh, Pennsylvania, June 2-5, 1974.

3. "Analysis of Hypothetical Core Disruptive Accident (HCDA)," GEAP-13921, General Electric Co. (July, 1972).

4. "Fast Flux Test Facility - Design Safety Assessment," HEDL-TM-72-92, Hanford Engineering Development Laboratory (July, 1972).

5. E. W. Bartes, L. W. Dietrich, J. G. Eberhart, A. K. Fischer and C. C. Meek, "Summary and Evaluation - Fuel Dynamics Lows and Flow Experiments," ANL-RAS--74-9, Argonne National Laboratory (June, 1974).

6. L. W. Dietrich, R. C. Doerner, T. H. Hughes, and A. E. Wright, "Summary and Evaluation - Fuel Dynamics Transient Overpower Experiments," ANL-RAS-74-8, Argonne National Laboratory (June, 1974).

7. D. E. Simpson, "The Hypothetical Core Disruptive Accident," lecture presented at the Massachusetts Institute of Technology Summer Course on Fast Reactor Safety, July 23-25, 1975.

8. S. D. Gabelnick and M. G. Chasanov, "A Calculational Approach to the Estimation of Fuel and Fission-Product Vapor Pressures and Oxidation States to 6000°K," ANL-7867, Argonne National Laboratory (October, 1972).

9. S. M. Zivi, M. Epstein, R. W. Wright, J. J. Barhusen, D. H. Cho, F. J. Testa, G. T. Goldfuss, and R. W. Mouring, "An In-Pile Study of Thermal Interaction Between High Energy Molten UO_2 Fuel and Liquid Sodium," *Nucl. Sci. Eng., 56,* 229-240 (1975).

10. R. W. Ohse, P. G. Berrie, H. G. Bogensberger, and E. A. Fischer, "Measurement of Vapour Pressure of (U, Pu)O_2 and UO_2 to 5000°K for Fast Reactor Safety Analysis and the Contribution of the Radial CS Distribution to Fuel Pin Failure," *Proceedings of a Symposium on the Thermodynamics of Nuclear Materials Held by the International Atomic Energy Agency at Vienna, October 21-25, 1974,* Vol. I, pp. 307-327.

11. M. Bober, H. U. Karow, and K. Schretzmann, "Evaporation Experiments to Determine the Vapour Pressure of UO_2 Fuel (3000-5000°K)," *Proceedings of a Symposium on the Thermodynamics of Nuclear Materials Held by the International Atomic Energy Agency at Vienna, October 21-25, 1974,* Vol. I, pp. 295-307.

12. M. Bober, H. U. Karow, and K. Schretzmann, "Vapor Pressure Measurements of Oxide Fuel Between 3000 and 5000°K Using Laser Heating," *Nucl. Technol., 26,* 237 (1975).

13. M. H. Fontana and T. S. Kress, "Liquid-Metal-Cooled Fast Breeder Reactor Safety," ORNL-TM-4914, Vol. III, Oak Ridge National Laboratory (July, 1975).

14. R. P. Anderson and D. R. Armstrong,"Laboratory Tests of Molten-Fuel-Coolant Interactions," *Trans. Am. Nucl. Soc., 15:1,* 313 (1972).

15. Hans K. Fauske, "On the Mechanism of Uranium Dioxide-Sodium Explosive Interactions." *Nucl. Sci. Eng., 51,* 95-101 (1973).

16. M. H. Fontana, "Core Melt-Through in LMFBR's - A Condensed Review," ORNL-TM-3504, Oak Ridge National Laboratory (September, 1971).

17. M. Epstein and D. H. Cho, "Fuel Vaporization and Quenching by Cold Sodium; Interpretation of Treat Test S-11," CONF-740401-P1, *Proceedings of the Fast Reactor Safety Meeting, Beverly Hills, California, April 2-4, 1974.*

18. A. B. Reynolds, M. F.Kennedy, and H. Honig, "Condensation of a Large Sodium Vapor Bubble After a Fast Reactor Disassembly Accident," *Trans. Am. Nucl. Soc., 14,* 738 (1971).

19. F. L. Horn and A. W. Castleman, Jr., "PuO_2-UO_2-Na Aerosols Produced by Vaporization of Fast Reactor Core Materials," BNL-12757, Brookhaven National Laboratory (October, 1968).

20. P. E. Blackburn, C. E. Johnson, I. Johnson, A. E. Morten, M. Tetenbaum, C. E. Crouthamel, A. D. Tevebaugh, and R. C. Vogel, "Chemical Engineering Division Fuels and Materials Chemistry Semiannual Report, July-December (1971)," ANL-7877, Argonne National Laboratory (April, 1972).

21. M. G. Adamson, "Oxygen Thresholds for the Sodium-Fuel Reactions; An Evaluation of Experimental Results," GEAP-12519, General Electric Co. (July, 1974).

22. M. G. Chasanov, C. E. Johnson, N. O. Dudey, P. E. Blackburn, M. J. Fluss, R. R. Heinrick, I. Johnson, A. E. Martin, M. Tetenbaum, C. E. Crouthamel, M. Levenson, R. C. Vogel, D. S. Webster, and L. Burris, "Chemical Engineering Division Fuels and Materials Chemistry Semiannual Report, January-June (1973)," ANL-8022, Argonne National Laboratory (December, 1973).

23. P. A. G. O'Hare, W. A. Shinn, C. F. Mrazek, and A. E. Martin, "Thermodynamic Investigation of Trisodium Uranium(V(Oxide (NA_3UO_4) I. Preparation and Enthalpy of Formation," *J. Chem. Thermodyn., 4,* 401-409 (1972).

24. E. A. Aitken, "Thermodynamic Analysis of Possible Chemical Interactions in the System: UO_2-PuO_2 Fuel-Sodium-Stainless Steel," GEAP-5683, General Electric Co. (July, 1968).

25. A. B. Reynolds, C. A. Erdman, P. L. Garner, P. M. Haas, and M. Kirbiyik, "Molten Material-Coolant Interaction and Plutonium Source in LMFBR Accident Analysis," ORO-4313-9, ORO-4313-10, Ninth and Tenth Quarterly Reports for December 15, 1973 - June 30, 1974, Oak Ridge Operations (September, 1974).

26. M. F. Kennedy and A. B. Reynolds, "Methods of Calculating Vapor and Fuel Transport to the Secondary Containment in a LMFBR Accident," *Nucl. Technol., 20,* 149 (1975).

27. D. R. Armstrong, F. J. Testa, D. Raridon, Jr., "Molten UO_2-Sodium Dropping Experiments," *Trans. Am. Nucl. Soc., 13,* 660 (1970).

28. R. L. Koontz and H. A. Morewitz, "An Evaluation of the Behavior of Aerosols Produced by the LMFBR DBA," AI-AEC-MEMO-12761 (REV.I), Atomics International (May, 1969).

29. T. R. Johnson, L. Baker, Jr., and J. R. Pavlik, "Large Scale Molten Fuel-Sodium Interaction Experiments," CONF-740401-P2, *Proceedings of the Fast Reactor Safety Meeting, Beverly Hills, California, April 2-4, 1974.*

30. M. D. Allen and J. K. Briant, "*Characterization of LMFBR Fuel-Sodium Aerosols,*" *Health Phys., 35,* 237-254 (1978).

31. W. A. Zanotelli, G. D. Miller, and E. W. Johnson, *1978 Annual Report: Aerosol Characterization from a Simulated HCDA,* NUREG/CR-0740, MLM-2597 (1978).

32. E. W. Johnson, D. L. Fleming, R. E. Zielinski, anad W. A. Zanotelli, *Annual Report: Aerosol Characterization from a Simulated HCDA,* MLM-MU-77-07-0004 (October 27, 1977), 27 pp.

33. P. E. Blackburn, "Reaction of Sodium with Uranium-Plutonium Oxide and Uranium Oxide Fuels," in *Behaviour and Chemical State of Irradiated Ceramic Fuels,* IAEA-PL-463/23, (1974), p. 393.

34. Q. E. Martin and J. Schilb, *ANL Fuels and Materials Chemistry Semiannual Report,* ANL-7977, Argonne National Laboratory, Chemical Eng. Div., (July-December 1972), pp. 4-9.

35. J. Sestak and G. Berggren, "Study of the Kinetics of the Mechanism of Solid-State Reactions at Increasing Temperatures," *Thermochim. Acta, 3,* 1-12 (1971).

36. G. N. Kelly, J. A. Jones and J. R. Simmonds, "The Influence of the Physio-Chemical Form of the Aerosol on the Radiological Consequences of National Accidental Releases of Radioactivity from a Fast Breeder Reactor," NRPB-R73, National Radiological Protection Board, January, 1979.

37. J. Brightwell and R. F. Carter, "Comparative Measurements of the Short-Term Lung Clearance and Translocation of PuO_2 and Mixed Na_2O + PuO_2 Aerosols in Mice, Inhaled Particles and Vapours IV," W. H. Walton, ed., Pergamon Press, Oxford, p. 285 (1977).

38. D. D. Mahlum, J. O. Hess and M. D. Allen, "Translocation of Mixed LMFBR Fuel-Sodium Aerosols from the Lung Following Inhalation by Rodents," Annual Report for 1977, Pt. 1, PNL 2500, Battelle Pacific Northwest Laboratories, Richland, Wash., p. 3.59 (1978).

39. D. R. Rogers, "Mound Laboratory Environmental Plutonium Study 1974," MLM-2249 (September, 1975).

40. R. L. Fleischer and O. G. Raabe, "Fragmentation of Respirable PuO_2 Particles in Water by Alpha Decay - A Mode of Dissolution," *Health Phys., 32,* 253-257 (1977).

41. O. G. Raabe, S. V. Teague, N. L. Richardson and L. S. Nelson, "Aerodynamic and Dissolution Behavior of Fume Aerosols Produced During the Combustion of Laser-Ignited Plutonium Droplets in Air," *Health Phys., 35,* 663-674 (1978).

42. M. D. Allen, J. K. Briant, O. R. Moss, E. J. Rossignol, D. D. Mahlum, L. G. Morgan, J. L. Ryan and R. P. Turcotte, "Dissolution Characteristics of LMFBR Fuel-Sodium Aerosols," *Health Phys., 40,* 183-193 (1981).

43. G. M. Kanapilly, O. G. Raabe, C. H. T. Goh, and R. A. Chimenti, "Measurement of In Vitro Dissolution of Aerosol Particles for Comparison to In Vivo Dissolution in the Lower Respiratory Tract after Inhalation," *Health Phys., 24,* 497-507 (1973).

44. O. G. Raabe, G. M. Kanapilly and H. A. Boyd, "Studies of the In Vitro Solubility of Respirable Particles of Pu-238 and Pu-239 Oxides and an Accidentally Released Aerosol Containing Pu-239," LF46, Inhalation Toxicology Research Institute Annual Report (1973).

45. C. C. Addison, M. G. Barker, R. N. Lithonbon and R. J. Pulham, "Reactions of Liquid Sodium with Transition Metal Oxides, Part III. The Oxides of UO_3 and U_3O_8," *J. Chem. Soc. A,* 2457-2459 (1969).

46. S. Jordan and Y. Ozawa, "Fuel and Fission Product Release from LMFBR-Core Catcher," CONF-761001-P4, 1924-1929 (1976).

47. J. W. Mausteller, F. Tepper and S. J. Rogers, "Alkali Metal Handling and Systems Operating Techniques," Gordon and Breach Science Publishers, Inc., New York (1967).

48. Miss Berlin, J. Colome and J. C. Malet, "Experimental Study of Sodium Fires on Concrete Based on the Sodium-Concrete Reaction and its Consequences: Study of the Behavior of Various Concretes under Metallic Sheaths," SANDS 77-6005, Sandia Corp. (April, 1977).

Distribution

EXTERNAL

Nuclear Regulatory Commission — R 7 (275)
H. N Hill, DOE, Dayton Area Office
R. K. Flitcraft, Monsanto Research Corporation
C. W. Roos, Monsanto Company, St. Louis
H. A. Schneiderman, Monsanto Company, St. Louis
Monsanto Reports Library, St. Louis

INTERNAL

W. R. Amos
L. R. Baird
C. E. Burgan
W. T. Cave
W. B. Cartmill
D. L. Coffey
J. K. Crawford
C. L. Fellers
V. L. George
C. J. Goebel
L. D. Haws
C. W. Huntington
E. W. Johnson
W. H. Jones
B. R. Kokenge
J. R. Marshall
G. D. Miller
D. L. Roesch
D. R. Rogers
D. R. Rohler
W. D. Sibert
R. E. Sprague
E. Stacy
D. B. Sullenger
R. E. Vallee
S. B. Wells
L. J. Wittenberg
W. A. Zanotelli (2)
R. E. Zielinski
Publications
Library (15)